

Modelling CO₂ and N₂O emissions from soils in silvopastoral systems of the West-African Sahelian band

Yélognissè Agbohessou^{1,2,3}, Claire Delon⁴, Manuela Grippa⁵, Eric Mougin⁵, Daouda Ngom¹, Espoir Koudjo Gaglo^{1,3}, Ousmane Ndiaye^{2,6}, Paulo Salgado^{7,8}, Olivier Roupsard^{3,9,10}

- 5 ¹Université Cheikh Anta Diop, Département de Biologie Végétale, Dakar, Senegal
²Institut Sénégalais de Recherches Agricoles, Dakar, Senegal
³LMI IESOL, Centre IRD-ISRA de Bel Air, Dakar, Senegal
⁴Laboratoire d'Aérologie, Université de Toulouse, CNRS, IRD, UPS, Toulouse, France
10 ⁵Géosciences Environnement Toulouse, Université de Toulouse, CNES, CNRS, IRD, UPS, Toulouse, France
⁶Centre de Recherches Zootechniques de Dahra, Institut Sénégalais de Recherches Agricoles, Dahra, Senegal
⁷CIRAD, UMR SELMET, F-34090 Montpellier, France
⁸UMR SELMET, University of Montpellier, CIRAD, INRAE, Institut Agro, F-34090 Montpellier, France
⁹CIRAD, UMR Eco&Sols, Dakar, Senegal
15 ¹⁰Eco&Sols, Univ Montpellier, CIRAD, INRAE, Institut Agro, IRD, Montpellier, France
- 15 *Correspondence to:* Yélognissè Agbohessou, (yelognissefredi.agbohessou@ucad.edu.sn)

Abstract. Silvopastoral systems (SPSs) have been shown to improve ecosystem resilience and provide sustainable land management solutions in the Sahel. However, accurately estimating the contribution of Sahelian ecosystems to the overall greenhouse gas (GHG) balance is a challenge, in particular the magnitude of carbon dioxide (CO₂) and nitrous oxide (N₂O) emissions from soils. In this work, we spatialized and applied the process-based model STEP-GENDEC-N₂O to investigate the magnitude, spatial, and temporal patterns of herbaceous mass, as well as CO₂ and N₂O emissions from soil (not net emissions) in Sahelian SPSs. Our results show that over the last decade (2012-2022), there was a heterogeneous spatial distribution of herbaceous mass production, as well as of soil CO₂ and N₂O emissions in Sahelian SPSs. Spatial variations in soil CO₂ emissions are primarily controlled by soil carbon content, temperature, herbaceous mass, and animal load, while soil nitrogen content, soil water content, and animal load are the main factors driving the spatial variations in N₂O emissions from soil. The estimated CO₂ and N₂O emissions from soil in Sahelian SPSs over the 2012-2022 period were equal to 58.79 ± 4.83 Tg CO₂-C yr⁻¹ (1 Tg = 10¹² g) and 21.59 ± 3.91 Gg N₂O-N yr⁻¹ (1 Gg = 10⁹ g), respectively. These values are generally lower than estimates reported in the literature for tropical areas and croplands. Furthermore, our simulations indicated a significant annual rising trend of soil CO₂ and N₂O emissions between 2012-2020 as herbaceous mass increases, making more C and N available for nitrification, denitrification and decomposition processes. By mapping soil CO₂ and N₂O emissions, we provide crucial insights into the localization of emission hotspots in Sahelian SPSs, thereby offering valuable information that can be used to devise and implement effective strategies aimed at fostering carbon sequestration in the Sahel.

Keywords: Sahelian Silvopastoral system, soil carbon dioxide emission, soil nitrous oxide emission, process-based model, greenhouse gas emission

1 Introduction

35 Carbon dioxide (CO₂) and nitrous oxide (N₂O) are two important greenhouse gases (GHG) that contribute significantly (>90%)
to anthropogenic climate warming (Hansen et al., 2000). With 298 times the warming potential of CO₂ over 100 years (Myhre
et al., 2013), N₂O is also a stratospheric ozone-depleting substance (Ravishankara et al., 2009). The atmospheric
concentrations of CO₂ and N₂O have experienced significant increases since the late 1700s (Bloch-Johnson et al., 2021; Prinn
et al., 2018). This surge is primarily attributed to emissions originating from terrestrial soils (Butterbach-Bahl et al., 2013;
40 Chevallier et al., 2015; Tian et al., 2020) during the period from 1700 to 1980 (Kammen and Marino, 1993). However, post-
1990, the major contributors to greenhouse gas emissions on a global scale shifted to the energy systems and industrial sectors
(Parmesan et al., 2022). CO₂ emissions from soil are due to organic matter decomposition (Robertson and Paul, 2000), while
N₂O is produced in soils through nitrification (*i.e.*, oxidation of ammonium to nitrate) and denitrification (*i.e.*, reduction of
nitrate to molecular N) (Davidson and Verchot, 2000). These processes are regulated by a range of environmental factors
45 (Aulakh et al., 1991; Bajracharya et al., 2000; Reth et al., 2005), making it difficult to up-scale soil CO₂ and N₂O emissions
from local sites to the regional and global scale.

Nevertheless, in the last decade, several works provided estimates of CO₂ and N₂O emissions from terrestrial soils at the large
scale (Dangal et al., 2020; Leahy, 2004; Tian et al., 2020, 2019, 2018, 2016, 2015). However, regions such as Africa, especially
West-African Sahelian livestock production systems have not received much attention. Our knowledge of the magnitude, and
50 the spatio-temporal distribution of soil CO₂ and N₂O emissions in these systems is limited and subject to large uncertainties
(Assouma et al., 2017). This is mainly due to a lack of experimental and modelling studies focused on the region.

Silvopastoral systems (SPSs) are one of the most common livestock production systems in the West-African Sahel (Le
Houerou, 1987; Herrero et al., 2013b, a; Turner et al., 2014). They are composed of a mix of trees and herbaceous cover,
grazed by livestock. As an attractive nature-based climate solution, SPSs offer long-term climate benefits thanks to the presence
55 of trees that have the potential to sequester carbon and offset GHG emissions (Agbohessou et al., 2023; Torres et al., 2017).
On the other hand, it has been reported that the livestock component of SPSs has an impact on the nitrogen (N) and carbon (C)
cycles and therefore on GHG emissions (Butterbach-Bahl et al., 2020). Indeed, livestock affects substrate availability in soil
through N input from their excreta, then impacting CO₂ and N₂O emissions (Butterbach-Bahl et al., 2020; Dangal et al., 2020).
It has been also reported that direct agricultural N₂O emissions from Africa mainly arise from livestock manure deposited in
60 pastures and rangelands (Xu et al., 2019). Livestock movements result in heterogeneous spatial and temporal distributions of
excreta, which increases spatial heterogeneity in soil properties and available nutrients which promote microbiological
processes driving soil CO₂ and N₂O emissions (Assouma et al., 2017; Smith et al., 2003). Actually, rangeland soils, combined
with livestock productions, were reported to be responsible for a large share of GHG emissions (Assouma et al., 2017; Soussana
et al., 2010; Valentini et al., 2014). The importance of rangelands in the global CO₂ and N₂O cycles and their potentialities to
65 increase atmospheric CO₂ and N₂O levels, have been highlighted in a number of studies (Chang et al., 2015; Dangal et al.,

2020; Leahy, 2004). Accordingly, to better understand the magnitude of GHG emissions in these systems and develop effective and spatially targeted climate solutions it is important to identify CO₂ and N₂O emission hotspots and accurately estimate emissions from Sahelian SPSs.

70 The different bottom-up approaches used to estimate large-scale soil CO₂ and N₂O emissions include the use of “emission factors” (EFs) as proposed by the Intergovernmental Panel on Climate Change (IPCC) (Hergoualc’h et al., 2019; IPCC, 2006), statistical extrapolation of field measurements, and process-based models (Bigaignon et al., 2020; Delon et al., 2019; Li et al., 2000; Parton et al., 2001). Besides, the top-down approaches integrate atmospheric measurements and atmospheric inversion models (Saikawa et al., 2014). Each method has its uncertainties and limitations, resulting in significant divergences in results across studies (Tian et al., 2019), especially in underrepresented regions like West-Africa (Tian et al., 2020). The IPCC defined N₂O emission as 1% of the applied N in the Tier 1 level (IPCC, 2006). This assumption of constant EF can neither depict spatial variations in N₂O emissions nor reflect the impacts of changing environments over time (Davidson and Kanter, 2014). Statistical extrapolation can also fail to depict the spatial heterogeneity in emissions, especially when the spatial variability in the parameters exceeds the conditions prevailing during the calibration step (Tian et al., 2019). On the other hand, the process-based model simulation approach has the advantage of describing the overall C and N cycle within the terrestrial systems and can integrate various driving factors controlling soil CO₂ and N₂O production and emissions (Tian et al., 2019). This approach involves the use of extensive data, such as meteorological, soil and ecosystem management data. However, estimating the model parameters can be challenging as there is a scarcity of experimental studies that encompass comprehensive details on local and regional pedoclimatic conditions and agricultural practices in West-Africa. Additionally, reliable and accurate large spatial scale input datasets for the models are often lacking, not only in under-represented areas but also in well-documented regions like Europe (Ballabio et al., 2016).

In this study, we selected the STEP-GENDEC-N₂O process-based model (Agbohessou et al., 2023), which couples water budget, herbaceous aboveground and belowground vegetation growth and decay, herbaceous and tree foliage litterfall (Jarlan et al., 2005; Mougin et al., 1995; Tracol et al., 2006), soil biogeochemistry and gaseous emissions (Bigaignon et al., 2020; Delon et al., 2019; Moorhead and Reynolds, 1991) to investigate the spatial and temporal patterns of herbaceous vegetation mass, CO₂ and N₂O emissions from soil, and estimate their annual budget in the Sahelian SPSs. The STEP-GENDEC-N₂O model was specifically designed for Sahelian semi-arid ecosystems and has been validated locally for soil CO₂ and N₂O emissions in several sites representative of the Sahelian SPSs (Agbohessou et al., 2023; Bigaignon et al., 2020; Delon et al., 2019, 2015). In this study, this model was upscaled and used at the regional scale, *i.e.* at the west Sahelian region scale.

The specific objectives of our study are to: (1) investigate the spatio-temporal patterns of herbaceous vegetation mass, CO₂ and N₂O emissions from soils in the Sahelian SPSs over the last decade (2012-2022); (2) identify the environmental factors responsible for the changes in the spatial patterns of soil CO₂ and N₂O emissions; and (3) estimate the soil CO₂ and N₂O budget of the Sahelian SPSs during the 2012-2022 period.

2 Materials and methods

2.1 Characteristics of the study area

100 The Sahel region is a semi-arid strip stretching across the African continent from Senegal to the red sea (Le Houérou, 1989). The region is characterized by high temperatures, low soil fertility and a long dry season alternating with a short rainy season, with precipitation occurring mostly between June and September, making it challenging to grow crops. As a result, a large portion of the region is used for pastoral activities, which serve as the primary means of subsistence (Touré et al., 2012). The focus of this study is put on Sahelian SPSs of West-Africa from longitude 18°W to 20°E and latitude 13°N to 18°N (Fig. 1 and A1), which cover approximately 40% ($\approx 892,353 \text{ km}^2$) of the Sahelian band. The dynamics of rainfall in the Sahel are strongly linked to the dynamics of the West African monsoon (Biasutti, 2019). The Sahel experienced a dry period from the late 1960s to the mid-90ies, marked by years of extreme droughts such as in 1973-1974 and 1984-1985. Several studies have reported a recovery period (Galle et al., 2018; Nicholson, 2017) for the Sahel since 1984, which is defined by an increasing trend in total seasonal rainfall (Biasutti, 2019; Dai et al., 2004). However, rainy season characteristics have changed; rainfall is more intense and intermittent (especially in areas with the lowest rainfall) and wetting is concentrated in the late rainy season (Biasutti, 2019; Chagnaud et al., 2022).

105

110

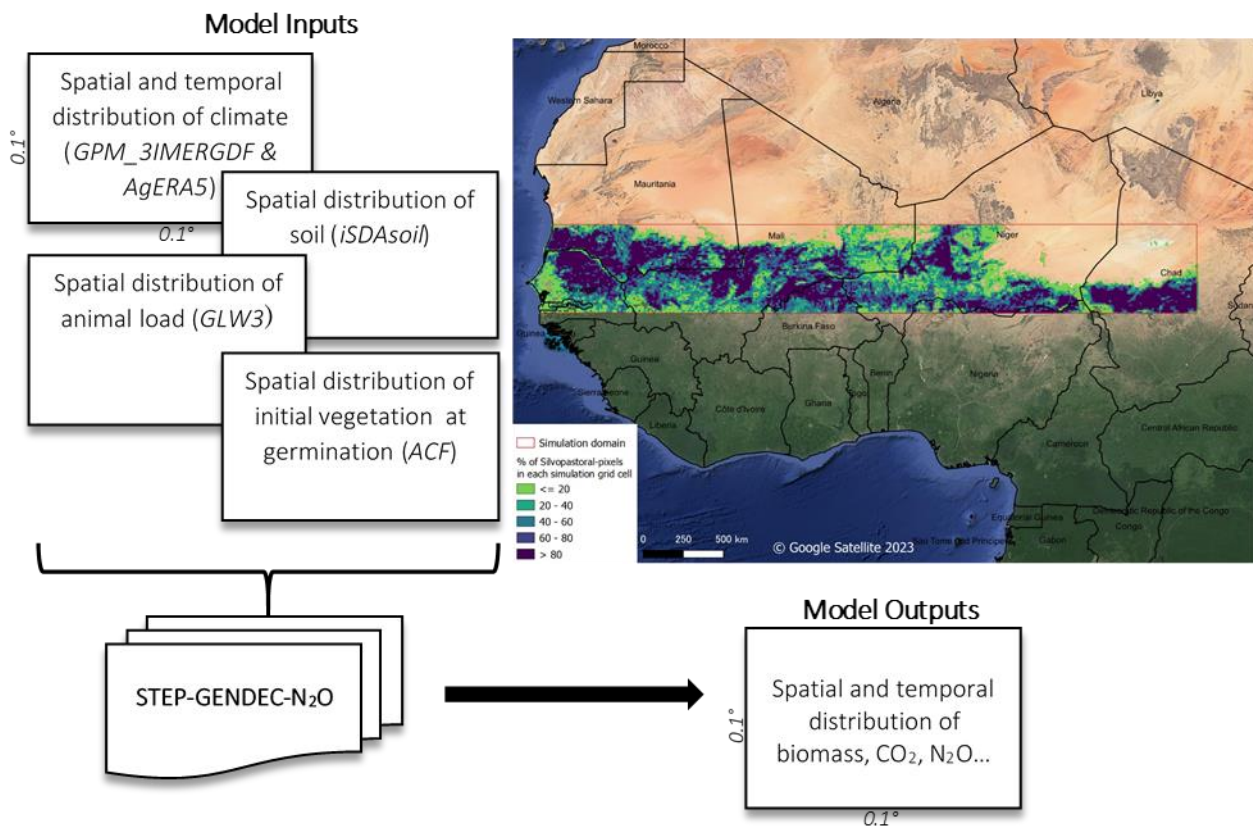


Figure 1: Illustration of the up-scaling approach used: model inputs and outputs and the simulation domain (Sahelian SPSs) are shown on the map. Silvopastoral areas were filtered from cultivated areas in the simulation area.

115 2.2 Model used from 1D processes to 2D up scaling: STEP-GENDEC-N₂O

2.2.1 Model description

STEP-GENDEC-N₂O is a process-based model developed for the Sahelian herbaceous savanna, coupling water budget, aboveground and belowground herbaceous vegetation growth and decay, litter fall (Mougin et al., 1995), soil biogeochemistry (Moorhead and Reynolds, 1991), and soil gaseous emissions (Agbohessou et al., 2023; Bigaignon et al., 2020; Delon et al., 120 2019). The model simulates the main processes describing the water, C, and N cycling between the atmosphere, vegetation, and soil at daily time steps and finally CO₂ and N₂O emissions. STEP-GENDEC-N₂O is forced daily by rain, global radiation, air temperature, wind speed, and relative air humidity. The model has been applied and evaluated to estimate herbaceous vegetation mass in Senegal, Mali (Mougin et al., 1995; Tracol et al., 2006), and Niger (Hiernaux et al., 2009), CO₂, NO, and N₂O emissions in Mali (Delon et al., 2015) and Senegal (Agbohessou et al., 2023; Bigaignon et al., 2020; Delon et al., 2019). 125 In the litter decomposition GENDEC sub-model, the soil C content is calculated from the total litter input provided by STEP while soil N is derived from the quantity of C using C/N ratios (Moorhead and Reynolds, 1991). Soil moisture, soil temperature, and biomass (*i.e.*, herbal aerial mass, herbaceous root mass, ligneous leaves mass and faecal matter by livestock) are used as input variables to simulate microbial respiration. This is done by examining the interaction between buried litter, decomposer microorganisms and six C and N pools (*i.e.*, labile compounds, holo-cellulose, resistant compounds, dead microbial biomass, 130 living microbial biomass and soil N). N₂O production and emissions from nitrification and denitrification are simulated using DNDC's (DeNitrification-DeComposition) equations (Li et al., 2000; Liu, 1996), adapted to the semi-arid region as described in Bigaignon et al. (2020) and Agbohessou et al. (2023). STEP alone has already been run to simulate aboveground biomass production, at the local scale (Jarlan et al., 2008, 2005, 2003; Mougin et al., 1995), meso scale (Grippa et al., 2017) and West-African Sahel scale (Pierre et al., 2016). Find in the appendices, the summary figure (Fig. A9) showing the connection between 135 the models STEP, GENDEC, and the N₂O module.

2.2.2 Model up-scaling

We used STEP-GENDEC-N₂O to simulate daily herbaceous vegetation mass, CO₂ and N₂O emissions from soil in West Sahelian SPSs. We developed a framework to run the model at a regional scale, using the parameterizations developed in the above-cited studies. Simulations were performed at the West Sahelian band scale (Fig. 1) divided into 18271 grid cells of 0.1° x 0.1°, from 2012 to 2022. Input variables were extracted from different datasets available at the global or regional scale as 140 described below (Table 1). For the soil dataset which is provided at finer resolution (<0.1° x 0.1°), pixel values for each centroid of the 18271 simulation grid cells were extracted. Simulations were performed over an 11-year period (2012-2022) preceded by a 6-year spin-up using the meteorological forcing data of year 2012, which was repeated 6 times. The spin up period allows for carbon and nitrogen pools to reach stability, as in Agbohessou et al. (2023). Indeed, in the model, the carbon

145 compartments for buried litter, feces, and dry roots are not initialized at 0, thus our simulations start with initial carbon values
of 3.7, 0.3, and 6.0 gC for buried litter, feces, and dry roots, respectively. These values represent means derived from in situ
measurements collected over several years at the Dahra site, where the model has been previously employed at the local scale.
The carbon and nitrogen submodel used is relatively simple, employing first-order differential equations with moderate
150 nonlinearity, which likely accounts for the rapid convergence observed in the model. All this explains why extensive spin-up
time is not necessary for running the model with appropriately supplied carbon and nitrogen compartments.

Table 1:

Summary of the datasets used for input variables and land cover/use

Dataset	Input variable (unit)	Spatial resolution	Temporal resolution	Ref	URL
iSDAsoil	Soil pH (-) and soil texture (clay, silt, and sand content (%))	30 m	01-01-2012 (taken as constant)	(Hengl et al., 2021)	https://developers.google.com/earth-engine/datasets/tags/isda?hl=en
ERA5-Land	Initial soil water content (mm) and initial soil temperature (°C)	0.1° x 0.1°	01-01-2012 (taken as constant)	(Muñoz Sabater, 2019)	https://cds.climate.copernicus.eu/cds/app#!/dataset/reanalysis-era5-land?tab=form
GPM_3IMERGDF	Precipitation (mm)	0.1° x 0.1°	01-01-2012 to 31-12-2021 (daily)	(Huffman et al., 2019)	https://disc.gsfc.nasa.gov/datasets/GPM_3IMERGDF_06/summary?keywords=%22IMERG%20final%22
AgERA5	Temperature (°C), Solar radiation (MJ m ⁻²), Vapour pressure (hPa), Wind speed (m s ⁻¹), Soil albedo (-)	0.1° x 0.1°	01-01-2012 to 31-12-2021 (daily)	(Boogaard et al., 2020)	https://cds.climate.copernicus.eu/cds/app#!/dataset/sis-agrometeorological-indicators?tab=overview
Gridded Livestock of the World version 3 (GLW3)	Animal load (-)	0.083333 decimal degrees	2012 (taken as constant)	(Gilbert et al., 2018)	https://dataverse.harvard.edu/dataverse/gld
Action Contre la Faim Surveillance West Africa	Proxy of herbaceous mass at germination (Kg ha ⁻¹)	1 km	2019-2021 (taken as constant)	(Lambert et al., 2019; Bernard and Fillol, 2020, 2021)	https://data.humdata.org/dataset/acf_biomass_west-africa_raster
Tree area density	Proxy of trees' foliar biomass	100 m	2023 (taken as constant)	(Tucker et al., 2023)	https://daac.ornl.gov/cgi-bin/dsvviewer.pl?ds_id=2117
Land Cove/Use product					
Global Land Cover – SHARE (GLC – SHARE)	Land cover and land use (-)	1-km	2013 (taken as constant)	(Latham et al., 2014)	https://data.apps.fao.org/map/catalog/srv/eng/catalog.search#/metadata/ba4526fd-cdbf-4028-a1bd-5a559c4bff38

2.3 Model input data

2.3.1 Climate data

155 The climate data required for the simulation were derived from two different datasets (GPM_3IMERGDF and AgERA5).
Precipitation (mm) data were taken from the IMERG (Integrated Multi-satellitE Retrievals for GPM) dataset,
GPM_3IMERGDF (Huffman et al., 2019). GPM_3IMERGDF or GPM IMERG Final Precipitation L3 1 day 0.1 degree x 0.1
degree V06, is derived from the half-hourly GPM_3IMERGHH dataset (Huffman et al., 2019) and represents the final estimate
of the daily accumulated precipitation. The selected product is “*precipitationCal**: multi-satellite precipitation estimates with
160 gauge calibration”. Dezfuli et al. (2017) validated the IMERG product in Africa using gauge data from West and East Africa.
They showed that the precipitation diurnal cycle is relatively better captured by IMERG than by the TMPA (TRMM Multi-
Satellite Precipitation Analysis) product. Maranan et al., (2020) did a process-based validation of GPM IMERG in Africa using
gauge data from a West African forested zone. Additionally, the choice of the IMERG dataset over the ERA5 dataset for
precipitation is based on expert recommendations and the results of previous evaluations of ERA5 precipitation data by Lavers
165 et al. (2022). Their study highlighted significant errors primarily in tropical regions. According to Lavers et al. (2022), users
can only have confidence in ERA5 precipitation data in extratropical regions.

The spatial distribution of the GPM_3IMERGDF average precipitation over the last decade (2012-2022) exhibits significant
gradients, with precipitation reaching as low as 0 mm at the northern border, exceeding 500 mm at the south-eastern border,
and exceeding 1000 mm at the south-western borders (Fig. A2). Additionally, there is a significant increasing trend in annual
170 mean precipitation amounts from 2010 to 2021, along with interannual variability (Fig. 3c).

Temperature ($^{\circ}\text{C}$), solar radiation (MJ m^{-2}), vapour pressure (hPa) and wind speed (m s^{-1}), were extracted from the AgERA5
dataset (Boogaard et al., 2020) using the R package “ag5Tools” (Brown and de Sousa, 2022). AgERA5 dataset provides daily
surface meteorological data matching the input needs of STEP-GENDEC- N_2O . The dataset is actually based on the ECMWF
(European Centre for Medium-Range Weather Forecasts) re-analysis ERA5-Land dataset (Muñoz Sabater, 2019). ERA5-Land
175 is an enhanced global dataset for the land component of the fifth-generation reanalysis produced by the ECMWF. It combines
extensive historical observations from satellites, aircraft, land and marine weather sensors into global estimates using advanced
modelling and data assimilation systems to generate consistent time series of multiple climate variables. More information
about ERA5-Land product can be found in Muñoz Sabater et al. (2021) and Gleixner et al. (2020). In the data used, no
significant trend ($p > 0.01$) was observed in average air temperature (range: $25\text{-}35^{\circ}\text{C}$), minimum air temperature (range: 16-
180 27°C), maximum air temperature (range: $25\text{-}39^{\circ}\text{C}$), global radiation (range: $19\text{-}25 \text{ MJ m}^{-2} \text{ d}^{-1}$), wind speed (range: $2\text{-}7 \text{ m s}^{-1}$)
and vapour pressure (range: $5\text{-}25 \text{ hPa}$) (extracted from ERA5-Land) in the Sahel between 2012 and 2022.

2.3.2 Soil data

185 Soil pH and soil texture (i.e. clay, silt, and sand content) were obtained from the iSDA (Innovative Solutions for Decision
Agriculture Ltd.) soil dataset (Hengl et al., 2021). The iSDAsoil dataset contains soil property predictions at 30 m pixel size
190 using machine learning coupled with remote sensing data and a training set of over 100,000 analysed soil samples all over
Africa (Hengl et al., 2021; Miller et al., 2021). Prediction uncertainty estimates per pixel for the iSDA soil properties data are
provided in Hengl et al. (2021). In the same study, the average accuracy performance based on fivefold spatial cross-validation
for various soil variables indicated that soil pH exhibited the highest performance with a concordance correlation coefficient
(CCC) of 0.90. The CCC values for soil clay content, sand content, and silt content were 0.85, 0.85, and 0.78, respectively.
We initialized the dry soil albedo, soil moisture (mm) and soil temperature (°C) at the beginning of the simulation using data
extracted from the ECMWF re-Analysis ERA5_Land (Muñoz Sabater, 2019).

195 Exploration of the extracted soil datasets showed that the soils in the Sahel region are typically sandy, with high levels of sand
and low levels of clay (Fig. A3a and A3b). This results in well-drained soils but low in nutrients. The soil pH in the south-
western part of the Sahel ranges from 5 to 7, while in the north and east it is higher than 7 (Fig. A3c). The pH levels of the
soils in the Sahel vary also depending on their texture. Sandier soils typically have a high pH (7-8.5), while clay soils have a
lower pH (5-7).

2.3.3 Animal load data

200 Information about livestock population and animal load distribution were obtained from the total livestock number for the
reference year 2010 provided by the Gridded Livestock of the World version 3 (GLW3) (Gilbert et al., 2018) dataset. GLW3
provides global population densities of cattle, buffaloes, horses, sheep and goats in each land pixel at a spatial resolution of
0.083333 decimal degrees (approximately 10 km at the equator). The relative spatial distribution of livestock over the
simulation period was assumed to be the same as the one indicated by the GLW3 database for the year 2010. To our knowledge
no measurement data are available on the temporal variation of livestock across the Sahel. Indeed, FAOSTAT provides
estimates of the livestock population at the national level for the period from 2012 to 2020 (FAOSTAT, 2024). However, these
205 data are only available at the national scale and have not been downscaled to the finer spatial scales required for our simulation.
GLW3 is currently the most recently compiled and harmonized subnational livestock distribution data available (and only
covers the year 2010). In Gilbert et al. (2018) it is mentioned that the outputs of the GLW3 dataset have been adjusted to ensure
that the total number of animals in a country aligns with the FAOSTAT 2010 total stock. There are no recent datasets available
prior to 2010 presenting livestock distribution at the subnational scale in our region to our knowledge. We used the annual
210 values of the GLW3 database to distribute the animal load on a monthly basis, taking into account the temporal variation of
the livestock population from one month to the next throughout the year. We assumed an increase of the livestock up to 100%
(in reference to the GLW3 database) in the pixels during the rainy season, and a gradual decrease down to 20% as we approach
the middle of the dry season.

215 Analysis of the GLW3 dataset revealed that livestock is heterogeneously distributed across the Sahel and the animal load is dominated by bovines, ovines, caprines and some equines (Gilbert et al., 2018). High livestock densities were observed in north-western Senegal, southern Mauritania, central Mali, northern Burkina-Faso, southern Niger, northern Nigeria and south-western Chad (Fig. A3f).

2.3.4 Initial biomass data

220 The model calibration input parameters related to herbaceous vegetation such as Initial mass (B_g0) and Initial Specific Leaf Area (SLA_g0) at germination date were computed using data from the biomass dataset provided by “Action Contre la Faim (ACF) Surveillance West Africa” (Bernard and Fillol, 2021, 2020; Lambert et al., 2019). ACF biomass data were produced from 10-day images of Dry Mass Production (DMP) from SPOT-VEGETATION 4&5, PROBA-V and SENTINEL-3 satellites (Lambert et al., 2019). The retrieval algorithm of the DMP product is described as follows (Monteith, 1972; Swinnen et al., 2022) Eq. (1):

$$225 \quad DMP = R \cdot fAPAR \cdot \varepsilon_{LUEc} \cdot \varepsilon_c \cdot \varepsilon_T \cdot \varepsilon_{CO2} \cdot CUE \quad (1)$$

DMP is the 10-day Dry Matter Production (kgDM/ha/day), R is the 10-day total shortwave incoming radiation (GJ_T/ha/day), $fAPAR$ is the PAR-fraction absorbed by green vegetation (J_{AP}/J_P), ε_{LUEc} is the light use efficiency at optimum (kgDM/GJ_{AP}), ε_c is the fraction of PAR in total shortwave (J_P/J_T), ε_T is the normalized temperature effect, ε_{CO2} is the normalized CO₂ fertilization effect and CUE is the carbon use efficiency.

230 The 1 km² resolution biomass raster product showing biomass production in the Sahel in kg ha⁻¹ yr⁻¹ was downloaded for the study period. We extracted the biomass value for each centroid of the simulation grid cells and performed a normalization by linearly scaling the dataset to a range between 0 and 2.5 g m⁻² (the min and max values of B_g0 in the STEP model) to get the spatial distribution of the initial biomass (B_g0) at germination date. To obtain the spatial distribution of the initial Specific Leaf Area (SLA_g0) at germination date, we normalized ACF biomass dataset to a range between 0 and 280 cm² g⁻¹ (min and max values of SLA_g0 given in Jarlan et al. (2008)). Here is the normalization formula used to linearly scale biomass values to B_g0 and SLA_g0 ranges Eq. (2):

$$235 \quad X_{norm} = a + \frac{(x - \min(x)) \cdot (b - a)}{x - \min(x)} \quad (2)$$

With X_{norm} representing the value of B_g0 or SLA_g0 , a and b being the smallest and the largest value that B_g0 or SLA_g0 can take, respectively, and x being the biomass values in the ACF dataset.

240 In the model B_g0 and SLA_g0 are calibration parameters. B_g0 mainly affects the date of peak biomass (Tracol et al., 2006), whereas SLA_g0 is used to estimate LAI (and $fAPAR$). The maximum conversion efficiency (ε_c) of absorbed radiation into biomass (i.e., g of dry matter per MJ of absorbed photosynthetically active radiation) was set to 5 g MJ⁻¹ which corresponds to the central value of the ε_c range possible values (Mougin et al., 1995; Pierre et al., 2011; Tracol et al., 2006) for all simulation grid cells.

245 2.3.5 Foliar mass of trees

Using the allometric equation developed by Hiernaux et al. (2023), we transformed the tree area density product provided by Tucker et al. (2023) into an estimate of tree foliar biomass in each simulation grid cell (Fig A3e). The conversion formula employed was Eq. (3):

$$DM_{foliar} = 0.2693 \cdot A^{0.9441} \quad (3)$$

250 Here, DM_{foliar} represents the mass of trees' leaves in kilograms, and A denotes the tree crown area in square meters.

2.4 Accounting for SPSs distribution in model outputs

Global Land Cover – SHARE (GLC – SHARE) dataset (Latham et al., 2014) provides information about the spatial distribution of a set of eleven major land cover classes (i.e., artificial surfaces, cropland, grassland, tree covered areas, shrubs covered areas, herbaceous vegetation, aquatic or regularly flooded, mangroves, sparse vegetation, bare soil, snow and glaciers, and water bodies) for the year 2013 and at 1-km² pixel resolution. First, we assumed that land cover change intensity was negligible in the Sahel during the last decade (the study period). Second, a new land cover class called silvopastoral areas was created and represents the sum of pixels of the classes: shrubs covered areas and grassland (Fig. 1).

The proportions of silvopastoral areas pixels within the 0.1° × 0.1° simulation grid cells (pixel resolution ≈ 123.21 km²) were calculated using the GLC – SHARE dataset to obtain the spatial distribution of silvopastoral systems in the Sahel (Fig. A1). In our analysis and interpretation of the spatial distribution of herbaceous mass, CO₂, and N₂O emissions, we consider the model outputs for simulation pixels where silvopastoral areas are > 80%. Additionally, bivariate maps were proposed, which display both model outputs and the distribution of SPSs in the simulation domain, to provide a more comprehensive view of the results.

To estimate the annual budget of soil CO₂ and N₂O emissions, the model outputs were weighted by the proportion of silvopastoral area within each simulation grid cell (Fig. 1 and Fig. A1), therefore considering all SPSs, even those which %SPS < 80%, across the simulation domain.

2.5 Random Forest algorithm for the analysis of soil CO₂ and N₂O emissions driving parameters

Random Forest (RF) is a machine learning method developed by Breiman (2001), it is a natural non-linear modelling tool that has proven valuable in many fields (Liu et al., 2022; Webb et al., 2021). We used the RF algorithm to identify the most important factors influencing the spatial distribution of soil CO₂ and N₂O emissions. The main advantages of RF algorithms are its low number of tunable factors, good tolerance to outliers and noise, general resistance to overfitting, and ability to identify and rank the most important variables (Liu et al., 2022; Webb et al., 2021). The RF algorithm was implemented into the R software (R Core Team, 2019) and the modelling framework provided by the *randomForest* R package (Liaw and Wiener, 2002) is used in our study. The target variables of the RF are the spatial distribution of the simulated soil CO₂ and soil

275 N₂O emissions, while the explanatory variables include the spatial distribution of various environmental and biological factors
susceptible to impact the spatial distribution of the soil CO₂ and N₂O emissions simulated by the STEP-GENDEC-N₂O model.
These factors consist of a combination of output variables from the STEP-GENDEC-N₂O model (e.g., soil water content, soil
temperature, soil C content, soil N content and herbaceous mass) and input variables for the STEP-GENDEC-N₂O model (e.g.,
280 soil sand content, soil clay content, soil pH, air temperature, albedo, annual precipitation and animal load). We conducted the
RF with the default parameters proposed by the *randomForest* package.

The method is composed of three critical steps, each of which plays a crucial role in the overall performance of the model. In
the first step, a bootstrap sample of observations (equal to the number of trees) is randomly drawn from the dataset, with
replacement. Approximately one third of the total observations are left out and used as "out-of-bag" (OOB) data to evaluate
the model's performance and prevent the need for a separate validation dataset (Efron and Tibshirani, 1986; Philibert et al.,
285 2013). This provides a resampling procedure that generates multiple versions of the training dataset, which helps to mitigate
overfitting and improves the accuracy of the model. In the second step, a random subset of predictor variables is selected at
each node of the decision tree (Ghattas, 2000; Philibert et al., 2013; Prasad et al., 2006). The number of variables selected
(mtry) was set to the integer part of the square root of the total number of variables (Breiman, 2001; Liaw and Wiener, 2002;
Philibert et al., 2013). This approach involves considering a subset of variables at each node of the decision tree and selecting
290 the best variable that maximizes the information gain. This randomization technique reduces the correlation among the trees
and makes the model more robust and accurate. In the final step, multiple decision trees are grown from the bootstrapped
dataset and the random subsets of features. The trees are grown using recursive binary partitioning of the data, with the best
split determined by optimizing a quality criterion such as information gain by the Gini impurity index (Breiman et al., 1984).
The final prediction is made by aggregating the predictions of all trees in the forest by averaging the outputs. The process is
295 repeated multiple times until a stable estimate of model performance is obtained.

We assessed variable importance using the percentage increase in Mean Squared Error (*%IncMSE*) after a factor was randomly
permuted. *%IncMSE* estimates the contribution of each variable to the reduction in the mean squared error of the model
(Breiman, 2001; Echeverry-Galvis et al., 2014). Factors with higher *%IncMSE* values are considered as more important in
explaining the spatial distribution of soil CO₂ and N₂O emissions. The importance of each factor was displayed with the
300 variable importance plot developed from the RF.

2.6 Statistical analysis and mapping

We conducted linear regression analysis to examine trends over time in herbaceous vegetation mass, soil CO₂ and N₂O
emissions and relevant emission driving variables. The Pearson correlation was used to assess the relationship between the
different variables. All statistical analysis and mapping were performed using R (R Core Team, 2019).

3.1 Spatio-temporal patterns of aboveground herbaceous mass in the Sahelian SPSs (2012-2022)

The annual production of aboveground herbaceous mass in the Sahelian SPSs, simulated from 2012 to 2022, displays a latitudinal gradient characterized by higher herbaceous mass in the southern regions, which diminishes as we progress towards the northern latitudes (Fig. 2). The same spatial pattern is observed in Figure 2b; which highlights results for Sahelian SPSs (pixel %SPS>80%). The maximum annual mean production (2012-2022) reaches 3 t DM ha⁻¹ yr⁻¹ and the annual minimum production is 0 t DM ha⁻¹ yr⁻¹.

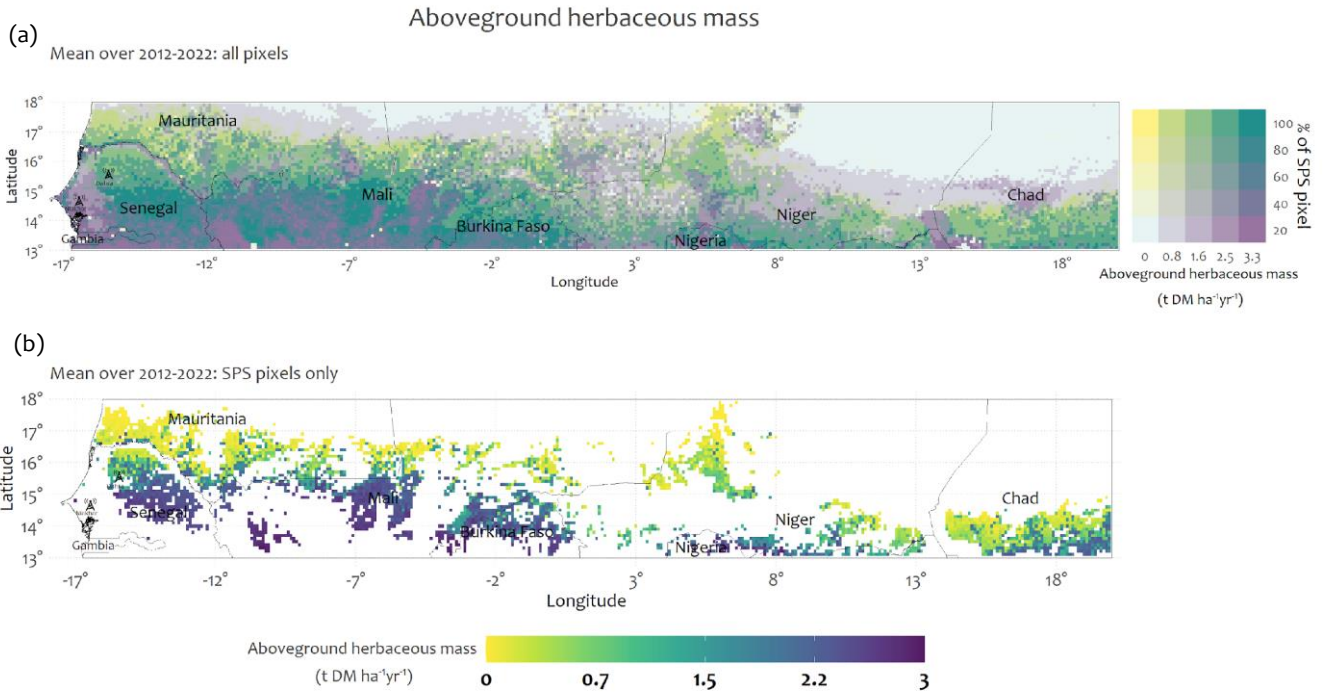
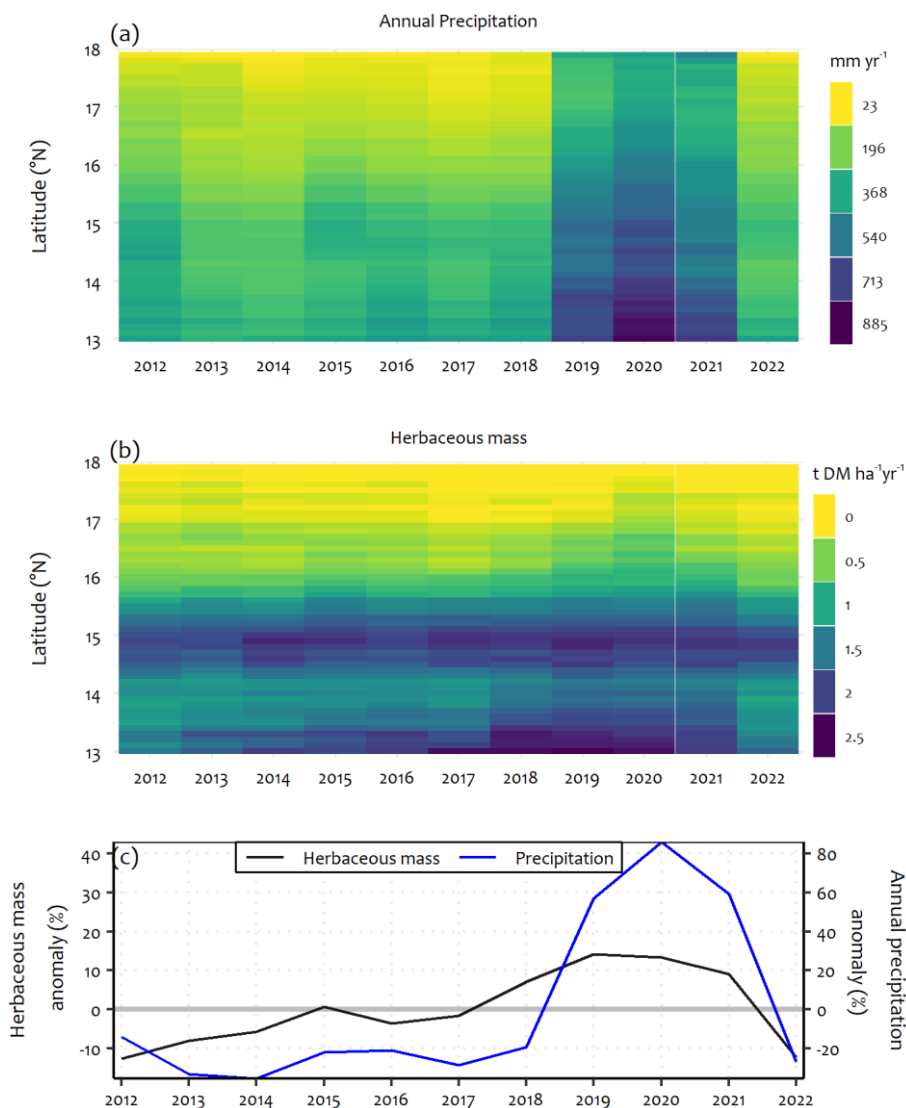


Figure 2: Regional distribution of simulated herbaceous mass in the Sahelian SPSs (annual mean over 2012-2022), in tDM ha⁻¹ yr⁻¹. (a) Bivariate map, which displays both simulated herbaceous mass and the distribution of SPSs in the simulation domain, (b) map filtering the simulated herbaceous mass for areas with Sahelian SPSs >80% only.

Herbaceous mass in Sahelian SPSs exhibited inter-annual variations with standard deviations reaching up to 1.3 t DM ha⁻¹ yr⁻¹ at some locations (Fig. A4a). We observed a significant increasing trend ($p < 0.001$) in the annual herbaceous mass anomaly (deviation from the 2012-2022 average) from 2012 to 2020 (Fig. 3a). This rising trend is evident in the Hovmöller representation, which depicts a gradual increase in herbaceous mass, particularly in the southern Sahel region around the latitudes 13°N and 15°N (Fig. 3b), with the highest production simulated in the wettest years (2019, 2020 and 2021, Fig. 3c). In the southern Sahel (13°N to 15°N), herbaceous mass in SPSs can reach 2.5 t DM ha⁻¹ yr⁻¹, while in the northern Sahel (16°N

to 18°N), it does not exceed 0.5 t DM ha⁻¹ yr⁻¹ (Fig. 3b). Overall, herbaceous mass in the Sahelian SPSs is highly correlated to the wet season total precipitation which shows large inter-annual variation (Fig. 3c: $p < 0.001$ and $r = 0.6$).



325

Figure 3: (a) Hovmöller (latitude-year) plot of the annual precipitation. (b) Hovmöller (latitude-year) plot of herbaceous mass in the domain indicated in Fig. 2b. (c) Interannual variations of anomalies (relative to the mean value for the period 2012-2022).

3.2 Soil CO₂ and N₂O emissions in Sahelian SPSs

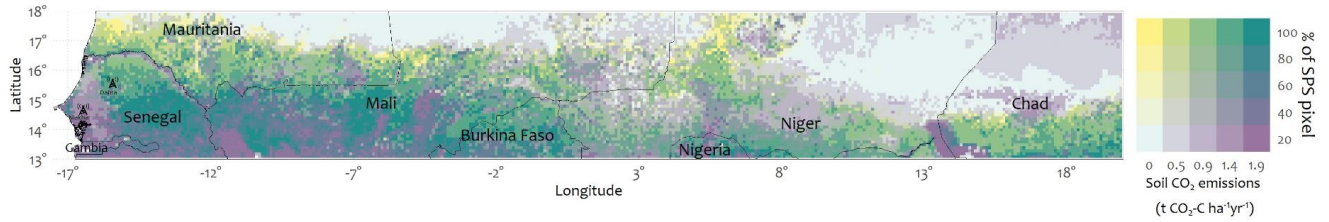
3.2.1 Spatial distribution across the Sahel

330 The simulation results reveal a heterogeneous spatial distribution of soil CO₂ and N₂O emissions, with the lowest emissions in the north and the highest emissions in the south (Fig. 4). SPSs in the pastoral zones of central Senegal, in southern and central Mali, in northern Burkina Faso, and in southern Niger (between longitudes 7°E and 8°E) exhibit high levels of soil CO₂ emissions (Fig. 4a and 4b). The average soil CO₂ emissions for the period 2012-2022, reached up to 1.7 t CO₂-C ha⁻¹ yr⁻¹, as shown in figure 4b. SPSs located in the northern regions of Niger, as well as in Mauritania, were generally not significant sources of CO₂ (Fig. 4b). Only SPSs of central Senegal, northern Burkina Faso and Mali remain constant CO₂ emission hotspots throughout the study period, with emissions as high as 2.6 t CO₂-C ha⁻¹ yr⁻¹ in some years, as shown in the all-years detailed maps in figure A6. Inter-annual variabilities of up to 0.7 t CO₂-C yr⁻¹ ha⁻¹ have been observed in some SPSs (Fig. A4b).

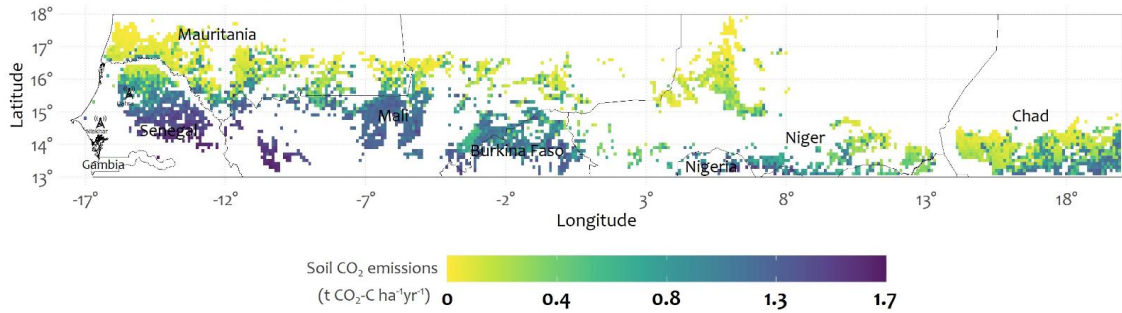
340 Figure 4c depicts heterogeneous soil N₂O emissions ranging from 0 to 3 kg N₂O-N ha⁻¹ yr⁻¹ and high emissions in some areas where the percentage of SPSs pixel is lower than 80%. The figure 4d exclusively show cases areas that are representative of the Sahelian SPSs (%SPS>80), showing that soil N₂O emissions were as high as 2.3 kg N₂O-N ha⁻¹ yr⁻¹ (mean 2012-2022 period) in SPSs located within the sandy pastoral zones of central Senegal, and in southern Mali between latitudes 13°N and 15°N. In contrast, smaller N₂O emissions were observed in the other SPSs of the region, especially in Niger and Chad. High inter-annual variabilities have been observed in the southern part of the Sahel (Fig. A4c).

Soil CO₂ emissions

(a) Mean over 2012-2022: all pixels

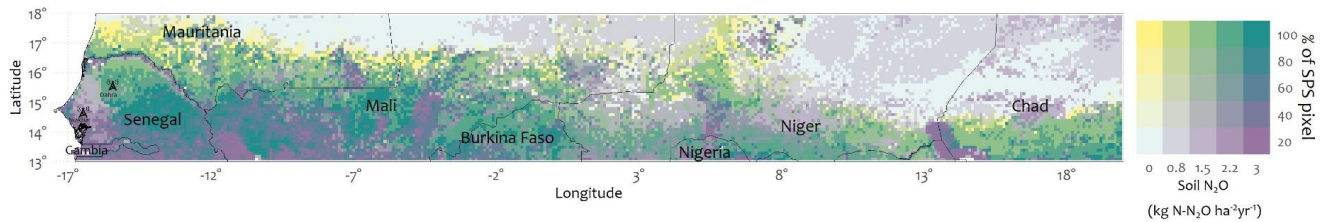


(b) Mean over 2012-2022: SPS pixels only

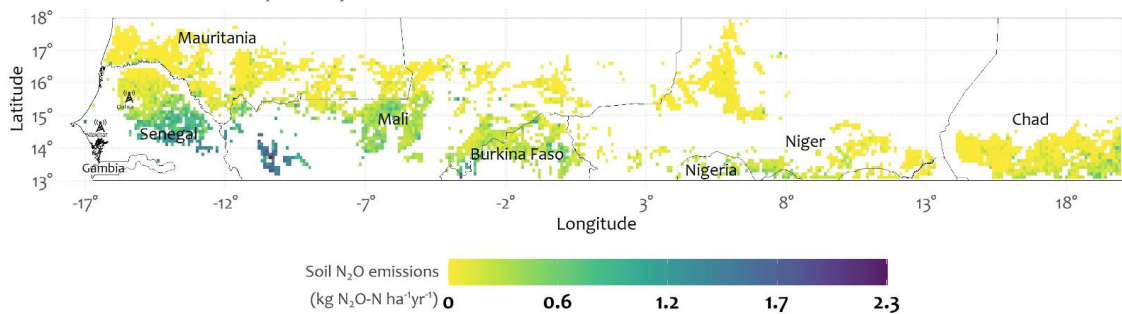


Soil N₂O emissions

(c) Mean over 2012-2022: all pixels



(d) Mean over 2012-2022: SPS pixels only



345

Figure 4: Regional distribution of simulated soil CO₂ and N₂O emissions in the Sahelian SPSs (annual means over 2012-2022). (a) and (c): Bivariate maps display both model outputs and the distribution of SPSs in the simulation domain. (b) and (d): Maps displaying model outputs only on areas representative of the Sahelian SPS (>80%).

3.2.2 Exploring the temporal dynamics of model outputs

350 Figure 5 shows the temporal dynamics of wet season precipitation, soil CO₂ emissions, soil N₂O emissions, soil water content and soil total C at two contrasted sites showing different emission levels (low and high), located in Niger (longitude 10.7, latitude 14.2) and Senegal (longitude -15.4, latitude 15.4) respectively. These sites were on predominant sandy soils. The observed dynamics of the different variables (precipitation, soil CO₂ emissions, soil N₂O emissions, soil water content and soil C content) at these sites show the model's ability to simulate realistically seasonal variations at fine time-scales in soil CO₂ and soil N₂O emissions in the Sahel.

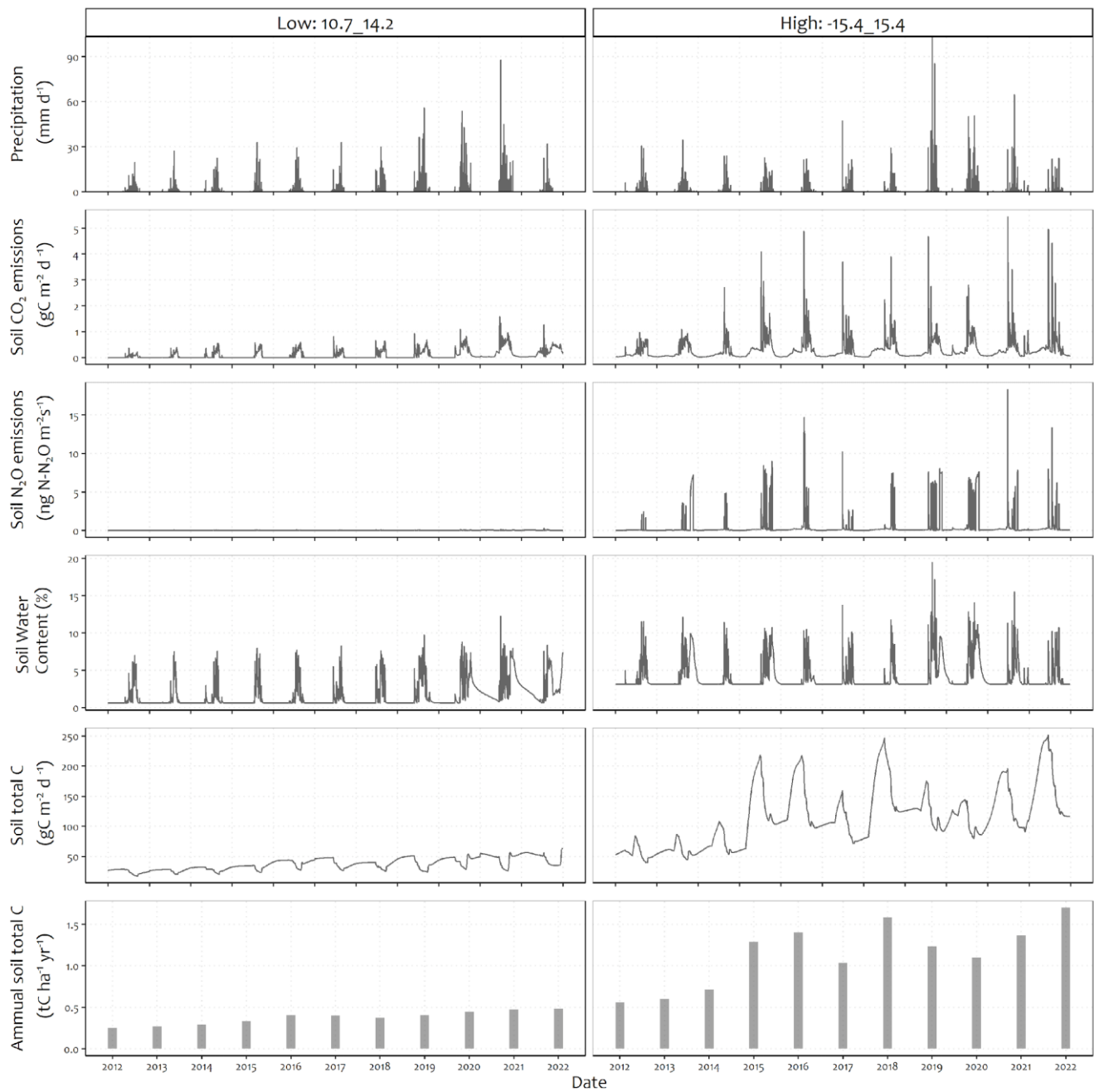
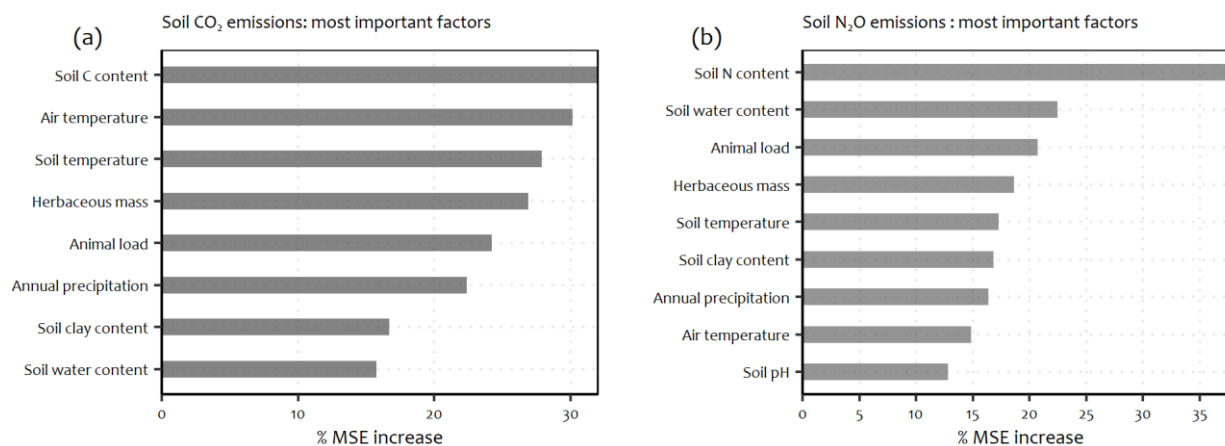


Figure 5: Temporal dynamics of model outputs across two sites with different levels of soil CO₂ & N₂O emissions. From top to bottom: precipitation, soil CO₂ emissions, soil N₂O emissions, soil water content and soil total C. At the left, a site exhibiting low emissions (latitude -10.7, longitude 14.2), at the right, a site with high emissions (longitude -15.4, latitude 15.4).

3.2.3 Factors controlling the spatial distribution of soil CO₂ and N₂O emissions

360 The observed variations in the spatial patterns of soil CO₂ and N₂O emissions were attributed to a complex interaction between meteorological, edaphic, bio-physical factors. According to a statistical analysis assessed by Random Forest over the model output in grid cells containing more than 80% of SPSs, the soil carbon and nitrogen contents were found to be the primary factors controlling the spatial distribution of soil CO₂ and N₂O emissions, respectively, as shown in figure 6. Soil C content, air temperature and soil temperature were identified as the three most significant factors controlling the spatial patterns of soil
365 CO₂ emissions. For soil N₂O, the two most significant factors after soil N content were soil water content and animal load. The results further showed that for soil CO₂, the other driving factors were herbaceous mass, animal load, annual precipitation (or soil water content), soil clay content, and soil water content (Fig. 6a). For soil N₂O, herbaceous mass, soil temperature, soil clay content, annual precipitation (or soil water content), and air temperature (in that order) also appeared as key driving factors (Fig. 6b). Soil pH was found to have the least influence on the spatial pattern of soil N₂O emissions (Fig 6).



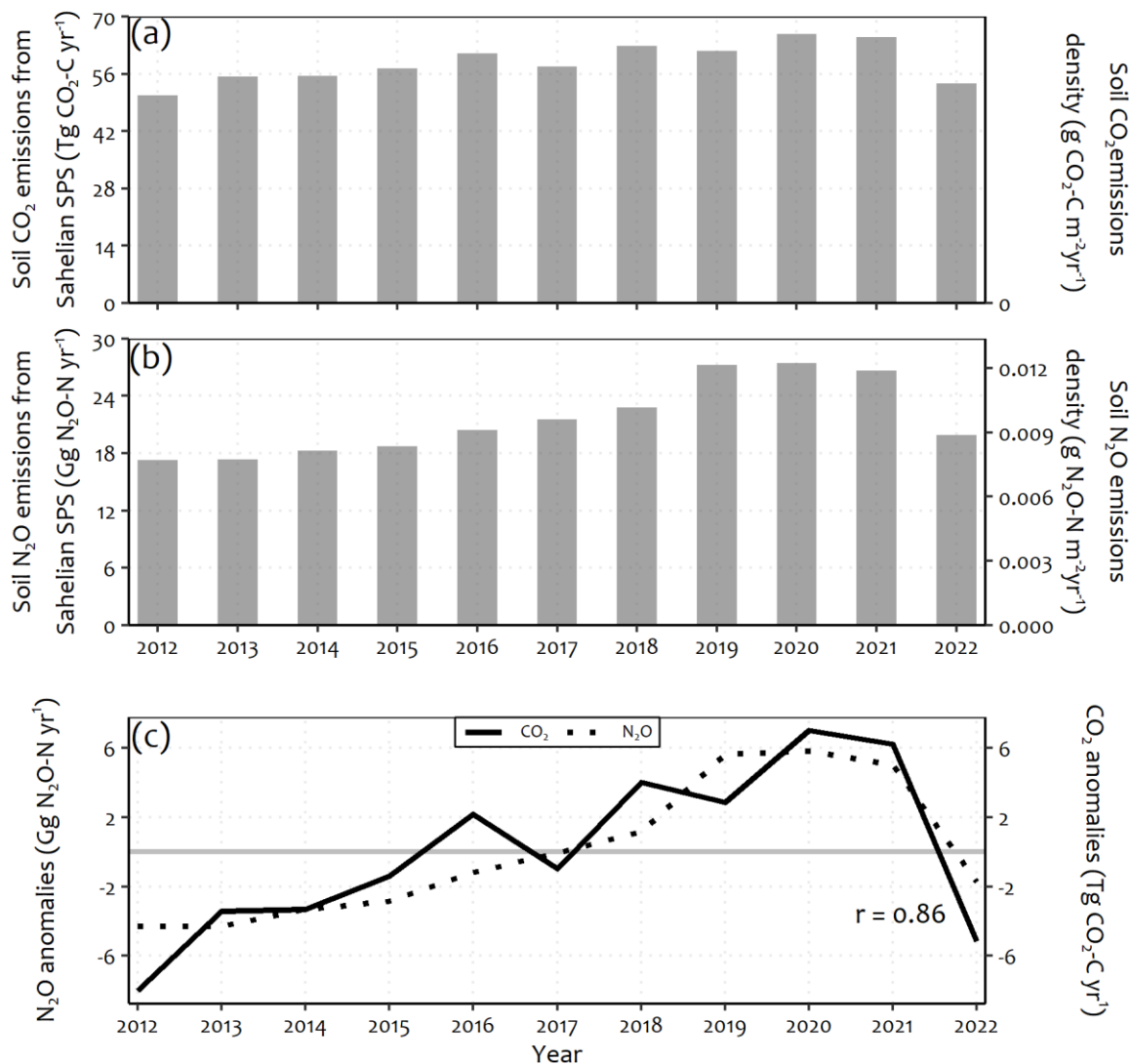
370

Figure 6: Factors controlling the spatial changes in (a) soil CO₂ and (b) N₂O emissions, from Random Forest Analysis. MSE = Mean Squared Error

3.2.4 Annual budgets across the Sahel (2012-2022)

375 The simulated soil CO₂ emissions include both microbial respiration and root respiration of herbaceous. Between 2012 and 2022, the estimated average soil CO₂ emissions in the Sahelian SPSs was 58.79 ± 4.83 Tg CO₂-C yr⁻¹ (1 Tg = 10¹² g). The highest soil CO₂ annual emission (65.80 Tg CO₂-C yr⁻¹) was found in 2020, while the lowest (50.77 Tg CO₂-C yr⁻¹) was in 2012 (Fig. 7a). During this same period, the mean soil N₂O emission was 21.59 ± 3.91 Gg N₂O-N yr⁻¹ (1 Gg = 10⁹ g), ranging from 17.31 Gg N₂O-N yr⁻¹ in 2012 to 27.43 Gg N₂O-N yr⁻¹ in 2020 (Fig. 7b). From 2012 to 2020, annual soil CO₂ and N₂O emissions showed significant ($p < 0.01$) rising trends of $4.30e-3 \pm 6.05e-4$ Tg CO₂-C yr⁻¹ and $3.75e-3 \pm 4.47e-4$ Gg N₂O-N yr⁻¹, respectively. However, emissions dropped after 2021, with a 17.5% decrease in soil CO₂ emissions and 25.5% decrease in
380 soil N₂O emissions (Fig. 7c). Figure 7c reveals that the inter-annual variations in soil CO₂ and soil N₂O emissions are quite

homothetic, as indicated by a Pearson's correlation coefficient of 0.86. Annual precipitation over the 2012-2022 period and averaged over the study domain was significantly correlated to both soil CO₂ ($p < 0.05$, $r = 0.48$) and N₂O ($p < 0.05$, $r = 0.79$) emissions.



385 **Figure 7: Interannual variation in soil CO₂ and N₂O emissions in the Sahelian SPSs (which covers approx. 892000 km²) during 2012-**
 390 **2022. (a) Soil CO₂ emissions in Tg C yr⁻¹ (1 Tg = 10¹² g) and (b) soil N₂O emissions in Gg C yr⁻¹ (1 Gg = 10⁹ g). (c) Interannual**
variations of soil CO₂ and soil N₂O anomalies (relative to the mean value for the period 2012-2022). The Pearson correlation
coefficient between CO₂ and N₂O anomalies was 0.86. We calculated the proportion of SPSs area pixels within each 0.1° x 0.1°
simulation grid cell, and used these values to weight the model outputs for each grid cell.

4 Discussion

Previous studies at global and regional scales have estimated greenhouse gas (GHG) emissions from various ecosystems, especially agricultural systems (Tian et al., 2020, 2015), forests (Tian et al., 2020; Verchot et al., 1999), and rangelands (Dangal et al., 2020). These studies have frequently highlighted significant uncertainties when estimating emissions from underrepresented regions, like in Africa. In addition, different modeling techniques often give divergent results when estimating emissions from these regions. In this study, we have up-scaled the 1D STEP-GENDEC-N₂O model, which was previously used in local studies across various sites in the West Sahel region. For example, in previous studies conducted at a SSP located in the northern region of Senegal (Dahra: 15°24'10"N, 15°25'56"W), Bigaignon et al. (2020) effectively used STEP-GENDEC-N₂O to satisfactorily simulate soil water content ($R^2 = 0.68$ & $RMSE = 1.67 \text{ mm d}^{-1}$), NO₃⁻ content in soil ($R^2 = 0.42$ & $RMSE = 0.83 \text{ mgN kgsoil}^{-1}$), and N₂O emissions ($R^2 = 0.36$ & $RMSE = 2.51 \text{ ng N m}^{-2} \text{ s}^{-1}$). At the same site, Agbohessou et al. (2023) successfully simulated CO₂ fluxes using STEP-GENDEC-N₂O combined with a tree growth model (DynACof (Vezy et al., 2020)), achieving convincing results for gross primary productivity (GPP: $EF = 0.49$ & $RMSE = 2.15 \text{ gC m}^{-2} \text{ d}^{-1}$) and ecosystem respiration (Reco: $EF = 0.56$ & $RMSE = 1.34 \text{ gC m}^{-2} \text{ d}^{-1}$). Additionally, Delon et al. (2019) demonstrated successful simulation of soil respiration on the identical site using STEP-GENDEC-N₂O. On another SSP located in Mali (Agoufou: 15.34° N, 1.48° W), Delon et al. (2015) employed STEP-GENDEC-N₂O to satisfactorily simulate soil moisture ($R^2 = 0.7$), soil temperature ($R^2 = 0.86$), and herbaceous mass ($R^2 = 0.72$), yielding satisfactory results. Building upon these previous local applications and validations of the STEP-GENDEC-N₂O model in different representative sites of the Sahelian SPS, we provide the first large-scale estimate of soil CO₂ and N₂O emissions from W-Sahelian SPS.

In this section, we discuss the magnitude of soil CO₂ and N₂O emissions reported in this study, the role of environmental and biological factors that drive the spatial heterogeneity observed in soil CO₂ and N₂O emissions in Sahelian SPSs, and the uncertainties and limitations associated with these estimations.

4.1 Spatial and temporal patterns of herbaceous vegetation, soil CO₂ emissions, and their relationship

In a previous study, Pierre et al. (2016) demonstrated the ability of the STEP model (alone) to simulate the dynamics of herbaceous vegetation at regional scale in the W-Sahel. They found a good agreement between the regional spatial patterns of STEP-simulated vegetation masses and the Moderate Resolution Imaging Spectroradiometer (MODIS) vegetation indices. They observed a latitudinal gradient in herbaceous vegetation mass, caused by the rainfall gradient, as also shown in our results. The magnitudes of herbaceous mass in their study and ours are comparable and the spatial patterns are similar although the study periods and the input data employed are not exactly the same. Previous estimates of mass production in the Sahel, using the LandscapeDNDC model (Rahimi et al., 2021) exhibited relatively stable temporal dynamics in mass production from 2010 to 2019. These estimates encompassed all land use types in the Sahel region, which could explain the divergence with our results showing a gradual increase in mass production in Sahelian SPSs between 2012 and 2022. Moreover, the trend observed in this study is mainly driven by the most recent years, with the highest values occurring in 2019, 2020 and 2021.

We compared the aboveground herbaceous mass (ABG) simulated by STEP-GENDEC-N₂O with the ABG biomass product from ACF (Bernard and Fillol, 2020, 2021; Lambert et al., 2019) for SPS pixels only (Fig. 8). This revealed a significant correlation between the ABG herbaceous mass simulated by STEP-GENDEC-N₂O and the ACF biomass product (with an R² value of 0.61 and an RMSE of 1.51). The ABG biomass derived from ACF amounts to 7 tDM ha⁻¹ yr⁻¹, whereas the simulated ABG herbaceous mass by STEP-GENDEC-N₂O does not exceed 3 tDM ha⁻¹ yr⁻¹. This variation can be attributed to the ACF product being derived from satellite data, encompassing not only herbaceous plants but also including the tree and crop component within these SPS-dominated pixels. Additionally, the Monteith formulation (Monteith, 1972) used by ACF approaches a potential biomass and therefore corresponds more to the upper bound of the STEP-GENDEC-N₂O simulations.

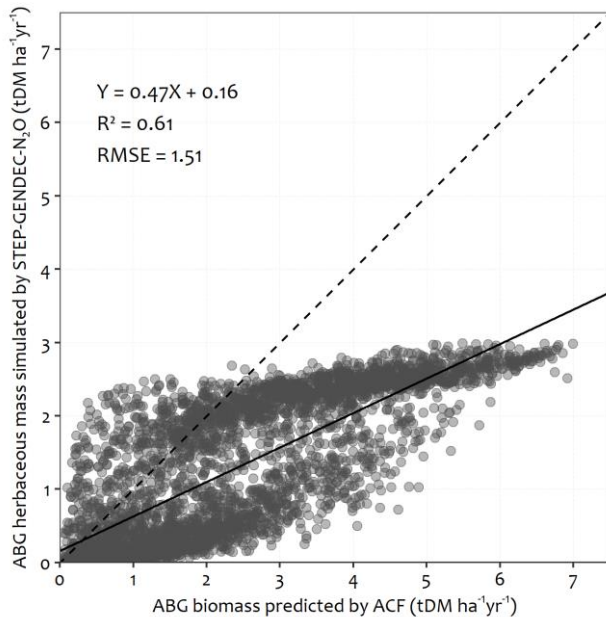


Figure 8: The relationship between aboveground (ABG) herbaceous mass simulated by STEP-GENDEC-N₂O and ABG biomass predicted by ACF (Bernard and Fillol, 2020, 2021; Lambert et al., 2019). Each point represents the annual mean biomass in a simulation pixel. The dashed line represents the 1:1 line, while the solid line depicts the linear regression line.

Plants' litter is the main source of carbon entering the soil, which explains the similar spatial patterns observed in both annual herbaceous mass (Fig. 2b) and annual soil CO₂ emissions (Fig. 4b). This illustrates the effect of the C substrate on CO₂ emissions, as confirmed by the Random Forest analysis (Fig. 6). The size and composition (nature of substrate, molecules, C/N ratio, etc.) of the available carbon pool actually control the magnitude of the CO₂ emissions from soil (Barnard et al., 2020). Soil CO₂ emissions include the respiration of soil microorganisms (microbial or heterotrophic respiration) and plant roots (autotrophic respiration), including all respiratory processes occurring in the rhizosphere (Raich and Potter, 1996; Xu and Shang, 2016). Root cells perform cellular respiration, metabolizing carbohydrates that are sent down from the leaves. Depending on the vegetation density, root respiration can contribute significantly to the total soil respiration (Macfadyen, 1970). In some SPSs in the north-western Sahel (*e.g.*, Mauritania, Mali and Niger), we simulated significant soil CO₂ emissions

445 despite the low herbaceous mass. These areas also exhibit high interannual variabilities in soil CO₂ emissions (Fig. A4b: up to
0.7 t CO₂-C ha⁻¹ yr⁻¹). The northern Sahel is generally characterized by a long dry season and very low rainfall. In such semi-
arid areas, at the onset of the wet season, the first rainfall events rewet the dry soil resulting in a mineralization peak leading
to a large soil CO₂ efflux pulse, also known as the “Birch effect” (Birch, 1958). The STEP-GENDEC-N₂O model accounts for
this “Birch effect” (Delon et al., 2019), which could explain the soil CO₂ emissions hotspots simulated in some SPSs of the
450 north-western Sahel. The site (simulation pixel) located at longitude -15.4°W and latitude 15.4°N (0.1 * 0.1 degrees), as
depicted in Figure 5, actually illustrates the Birch effect in soil respiration dynamics, with notably high emissions simulated at
the onset of the rainy seasons. This simulation pixel encompasses the Dahra site in northern Senegal (longitude -15.43222°W
and latitude 15.40277°N), where the 1D STEP-GENDEC-N₂O model results were in good agreement with observations
(Agbohessou et al., 2023; Delon et al., 2019). According to Fan et al. (2015), up to 20% of the annual soil CO₂ emissions to
455 the atmosphere occurs in African savanna ecosystems following intense rainfall. The CO₂ pulses associated with rewetting can
represent a large part of the annual C budget in semi-arid and arid ecosystems (Barnard et al., 2020; Jarvis et al., 2007; Ma et
al., 2012; Rey et al., 2017).

In a SPSs located in northern Senegal, Delon et al. (2017) measured soil respiration ranging from 2.4 ± 0.62 gC m⁻² d⁻¹ at the
onset of the wet season to 0.7 ± 0.01 gC m⁻² d⁻¹ at the end of the wet season in 2013. Our estimated mean soil CO₂ emissions
460 density for Sahelian SPSs between 2012 and 2022 (0.06 gC m⁻² d⁻¹) is lower than estimates at the global scale for grasslands
(2.2 gC m⁻² d⁻¹) and partially vegetated deserts (1.0 gC m⁻² d⁻¹) by Xu and Shang (2016). On a global scale, for these grasslands,
the substrate (soil C content) is probably much more important than in SPSs, which explains the higher values of CO₂
emissions. Our simulated soil CO₂ emissions for our region are also lower than the estimates by Warner et al. (2019). The soil
CO₂ emissions (soil respiration) calculated for our region (our simulation grid cells) from the Warner et al. (2019) product
465 indicate values as high as 7.8 tC ha⁻¹ yr⁻¹, whereas the simulated soil CO₂ emissions by STEP-GENDEC-N₂O do not exceed 2
tC ha⁻¹ yr⁻¹. These differences can be explained by the following points: (i) The Warner et al. (2019) product is a one-time
prediction based on input data from 01-01-1963 to 31-12-2011, while our simulated soil CO₂ emissions used for comparison
represent the annual mean of the period from 2012 to 2022. (ii) We used a process-based model (STEP-GENDEC-N₂O), while
the soil CO₂ emissions (soil respiration) predicted by Warner et al. (2019) are based on a machine learning approach,
470 specifically a quantile regression forest model. This model was trained using selected environmental predictors and 2,657 input
soil respiration observations from the global soil respiration database (SRDB) (Bond-Lamberty and Thomson, 2010).
However, it's important to note that the SRDB database used by Warner et al. (2019) does not contain measurements from
sites located in our region (the simulation area). Additionally, Warner et al. (2019) mentioned that the greatest prediction
uncertainties were observed in semi-arid ecosystems.

4.2 Soil N₂O and CO₂ emissions in Sahelian SPSs and importance of livestock

Between 2012 and 2022, the simulated soil N₂O emissions from Sahelian SPSs were 0.022 ± 0.004 Tg N₂O-N yr⁻¹. The regional natural soil N₂O emissions in Africa was estimated at 1.6 Tg N₂O-N yr⁻¹ for the period 2007-2016 (Tian et al., 2020). The simulated average soil N₂O emissions from Sahelian SPSs is lower than the median total N₂O emissions of 0.05 Tg N₂O-N yr⁻¹ from bomas (livestock enclosure where livestock excreta accumulate) in sub-Saharan Africa's semi-arid and arid climates (Butterbach-Bahl et al., 2020). The average soil N₂O emission density (per unit area) in Sahelian SPSs (2012-2022) was found to be 0.01 g N₂O-N m⁻² yr⁻¹ (range: 0-0.23 g N₂O-N m⁻² yr⁻¹), which is comparatively lower than the average estimate in tropical regions (0.11 ± 0.02 g N₂O-N m⁻² yr⁻¹) and the global average (≈ 0.05 g N₂O-N m⁻² yr⁻¹) reported for the period 2007-2016 (Tian et al., 2019). The soil N₂O emission density in Sahelian SPSs (2012-2022) was also lower than global emission densities estimated in croplands (0.21 ± 0.08 g N₂O-N m⁻² yr⁻¹) and other ecosystems (0.06 ± 0.01 g N₂O-N m⁻² yr⁻¹), respectively, during the period 2007-2016 (Tian et al., 2019). The most significant soil N input in Sahelian SPSs actually originates from livestock excreta, which is lower than the N input in most fertilized agricultural fields (Dangal et al., 2020), explaining the lower emission density in SPSs compared to the global average emissions density in croplands. In fact, studies have shown that nitrogen fertilizer application in croplands is the leading factor responsible for the increases in emission from agriculture (Cao et al., 2018; Davidson, 2009; Maavara et al., 2019; Shcherbak et al., 2014; Yao et al., 2020), followed by a minor yet significant rise in emissions from livestock manure (Tian et al., 2020). But on the other hand, in regions where very little nitrogen fertilizer is used in cropland such as in Africa, soil N₂O emissions mainly arise from livestock manure deposited in pastures and rangelands (Butterbach-Bahl et al., 2020; Dangal et al., 2020; Xu et al., 2019). This confirms the N₂O emission hotspots simulated in locations where the density of livestock is high (Fig. 4c & 4d, Fig A3f), as also highlighted by the Random Forest analysis. Indeed, the animal load distribution also affects the spatial distribution of soil N₂O and CO₂ emissions, as shown in figure 6. Several authors have already mentioned this impact (Assouma et al., 2017; Butterbach-Bahl et al., 2020; Dangal et al., 2020; Smith et al., 2003). Livestock influences the spatial distribution of soil C and N, which, in turn, significantly affects soil N₂O and CO₂ emissions.

4.3 Common features of soil CO₂ and N₂O emissions in Sahelian SPSs

Figure 7c shows that the inter-annual variations in soil CO₂ and soil N₂O emissions are quite homothetic, as indicated by a Pearson's correlation coefficient of 0.86. This suggests that they are both responding in a similar manner to the different ecological drivers. Some authors stated that the main processes responsible for CO₂ (decomposition) and N₂O (nitrification and denitrification) emissions from soils are influenced by the same environmental factors, namely soil moisture, soil temperature, soil texture, soil C and N content (Davidson and Swank, 1986; Oertel et al., 2016; Rastogi et al., 2002; Signor and Cerri, 2013). Several studies have shown how soil CO₂ and N₂O emissions evolve over time in response to changes in environmental driving factors (Cuhel et al., 2010; Davidson and Swank, 1986; Khalil, 2015; Ray et al., 2020) but the complexity of the interactions between these different factors make it difficult to assess the importance of each driver

responsible for the spatial distribution of the emissions. From our results, the main factor responsible for the spatial distribution of soil CO₂ and N₂O emissions in SPSs (Fig. 6) is substrate availability (soil C and N content), which outweighs other factors such as soil water content, temperature, and soil texture. Moreover, substrate availability is directly linked to herbaceous mass productivity (as mentioned in section 4.1) and to animal load (see section 4.2). This is consistent with the findings of Ray et al. (2020), who showed that soil CO₂ emissions are affected more by substrate availability than by rainfall, although their experiment was performed in a cropping system. In addition to influencing the spatial pattern of soil CO₂ and N₂O emissions, soil C and N also impact the temporal variation of these emissions, as shown in figure 5, where the largest emissions are found where the C content was the highest. Furthermore, our simulations revealed a rise in emissions between 2012 and 2020 (Fig. 7c), that is correlated to the increase in herbaceous mass during the same period (Fig. 3a). Indeed, the results produced by the Random Forest approach (Fig. 6) confirm our expectations regarding the soil C and N content as the primary factor influencing the spatial distribution of CO₂ and N₂O emissions from soils. The RF classification may solely originate from the hypothesis and the structure of the STEP-GENDEC-N₂O model if we were working at a local scale. However, since we are operating at a regional scale and the data inputted into the RF model reflect the spatial distribution of the explored factors in the region, we can attribute the RF classification, our result (Fig. 6), to a combination of the STEP-GENDEC-N₂O model's structure and the specific biophysical/edaphic conditions prevalent in the Sahelian band under investigation.

In the literature, soil water content is often highlighted as the major driver of the temporal variation of soil N₂O emissions as it regulates the oxygen availability to soil microbes (Butterbach-Bahl et al., 2013; Davidson and Verchot, 2000). The effect of soil moisture is actually predominant on denitrification processes, which lead to large amounts of N₂O emissions when soil water-filled pore space (WFPS) reaches 70 to 80% (Davidson and Verchot, 2000). This is consistent with the result of our RF analysis, which ranks soil water content as the second most important factor responsible for spatial changes in soil N₂O emissions (Fig. 6b). The impact of air temperature and soil temperature on the spatial distribution of soil CO₂ emissions suggests a positive feedback loop between climate warming and these emissions. The impact of global change drivers such as temperature on ecosystem processes and greenhouse gas emissions has been well studied and proven (Aulakh et al., 1992; Bajracharya et al., 2000; Lloyd and Taylor, 1994; Ray et al., 2020). The annual budgets of CO₂ and N₂O emissions (Fig. 7a and 7b) throughout the period of simulation show a low interannual variability. This can be attributed to the low interannual variability of influencing factors such as substrate availability (C: $33.60 \pm 2.38 \text{ gC m}^{-2} \text{ d}^{-1}$ N: $5.89 \pm 0.46 \text{ gN m}^{-2} \text{ d}^{-1}$), and soil water content ($4.87 \pm 0.19\% \text{ yr}^{-1}$). Our simulation results do not allow us to explore possible interactions between climate warming and annual soil CO₂ and N₂O emissions, as the average annual air temperature (averaged over the study domain) did not vary much over the simulation period ($28.37 \pm 0.25 \text{ }^\circ\text{C}$). Regional-scale observations show a temperature increase ranging from 1 to 2°C between 1950 and 2010 (Guichard et al., 2020). Therefore, over a 10-year period, this corresponds to a maximum increase of approximately 0.33°C, which is less than 0.5°C. This order of magnitude is comparable to the one computed for air temperature from the climate dataset used, and it is too small to be detected by temperature-versus-time regression.

4.4 Uncertainties and limitations

540 The lack of comprehensive dataset on the annual spatial distribution and growth dynamics of the livestock population in the Sahel between 2012 and 2022 remains a significant source of uncertainty in the CO₂ and N₂O emissions reported in this study. Actually, information on the spatial distribution and population of livestock was only available for the 2010 year (Gilbert et al., 2018). Only the spatial and the seasonal variability of the grazing pressure was taken into account in our simulation. We assumed that the annual distribution and growth dynamics of livestock in Sahelian SPSs did not change significantly between
545 2010 and 2022, although it might have been affected by the interannual variability of herbaceous mass. Given the significant impact of livestock on CO₂ and N₂O emissions in these ecosystems (Agbohessou et al., 2023; Assouma et al., 2017; Soussana et al., 2010; Valentini et al., 2014), an increase in livestock population during the study period could result in the misestimation of soil CO₂ and N₂O emissions. Significant changes in the spatial distribution of animal load from one year to another could also lead to some uncertainties in the simulated spatial distribution of the emissions. Furthermore, it's worth noting that our
550 estimate does not account for tree root respiration, which can lead to an underestimate of the total soil CO₂ emissions in regions with high tree density.

In a previous study employing the STEP-GENDEC-N₂O model at the local scale (within a silvopastoral system located in Senegal), Agbohessou et al. (2023) conducted an uncertainty analysis for STEP-GENDEC-N₂O using a Monte Carlo simulation and a sensitivity analysis with Sobol's method (Sobol, 2001). In this study, they evaluated the overall uncertainty
555 surrounding CO₂ and N₂O emissions simulated by STEP-GENDEC-N₂O and identified the key parameters/variables to which the CO₂ and N₂O emissions simulated by STEP-GENDEC-N₂O are most sensitive. They found that the CO₂ and N₂O emissions simulated by STEP-GENDEC-N₂O at the local scale are particularly sensitive to soil texture. This being the case, another significant source of uncertainty in the CO₂ and N₂O emissions reported in this study arises from the accuracy of the different input datasets used, especially the soil and precipitation datasets. We used the best dataset available for our region (to our
560 knowledge) for all input variables. However, the accuracy of our estimate also depends on the accuracy of the input dataset used. The choice of the various input datasets in this study is based on expert recommendations, comparison of the results of uncertainty analyses conducted for the different datasets in their respective reference articles, and their availability for our study region.

The soil C and N contents are significant factors influencing the spatial distribution of soil CO₂ and N₂O emissions in Sahelian SPSs, as indicated by our RF analysis. However, despite the availability of some local measurement data (Elberling et al.,
565 2003a, b) and databases related to soil C and N content (Hengl et al., 2021) in the Sahel region, accurately assessing the temporal variability of these elements in Sahelian SPSs soils remains challenging.

Finally, we assumed that natural or anthropogenic disturbances such as wildfires in Sahelian SPSs during our simulation period are fairly negligible. Uncertainties related to disturbances like wildfire are actually difficult to estimate as there are varying

570 perspectives and conflicting findings in the literature regarding the impact of burning on N₂O emissions (Karhu et al., 2015; Takakai et al., 2006).

5 Conclusions and perspectives

Our study advances the understanding of the spatial distribution and annual budget of CO₂ and N₂O emissions from soil in the Sahel. Information on the magnitude of CO₂ and N₂O emissions from soils in underrepresented areas are actually important to shed light on the contribution of these areas to the overall GHGs budget and thereby inform the development of effective mitigation strategies that can help reduce GHG emissions. SPSs represent a significant portion of the West African drylands, where they have expanded due to global warming and are expected to continue expanding in the near future (Thornton and Herrero, 2015). Previous studies at the local scale in the Sahel have shown that soils in semi-arid ecosystems are notable contributors to GHGs emissions (Assouma et al., 2017; Brümmer et al., 2009; Delon et al., 2017). Our results extended these local estimates to a broader spatiotemporal scale, showing that, overall, Sahelian SPSs soil emits less CO₂ and N₂O than tropical areas and croplands, on a global scale. Furthermore, by mapping emissions we provided crucial insights into the localization of soil CO₂ and N₂O emission hotspots, thereby offering indirect assessments of soil health in the Sahel region. This information can be a valuable asset for land managers who can leverage it to devise and implement effective strategies aimed at minimizing emissions and fostering carbon sequestration.

585 To further refine estimates of soil CO₂ and N₂O emissions in Sahelian SPSs, efforts to collect comprehensive datasets on livestock spatial distribution and temporal dynamics, tree densities and fire are needed. Additionally, more experimental studies should investigate the roles of nitrification and denitrification processes for soil N₂O emissions and the role of the decomposition process for CO₂ emissions in semi-arid ecosystems to better parameterize the model.

6 Appendices

590 Appendix A:

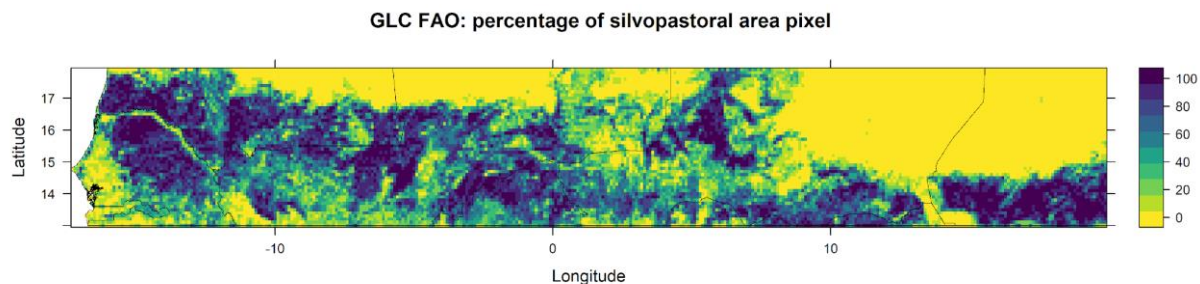
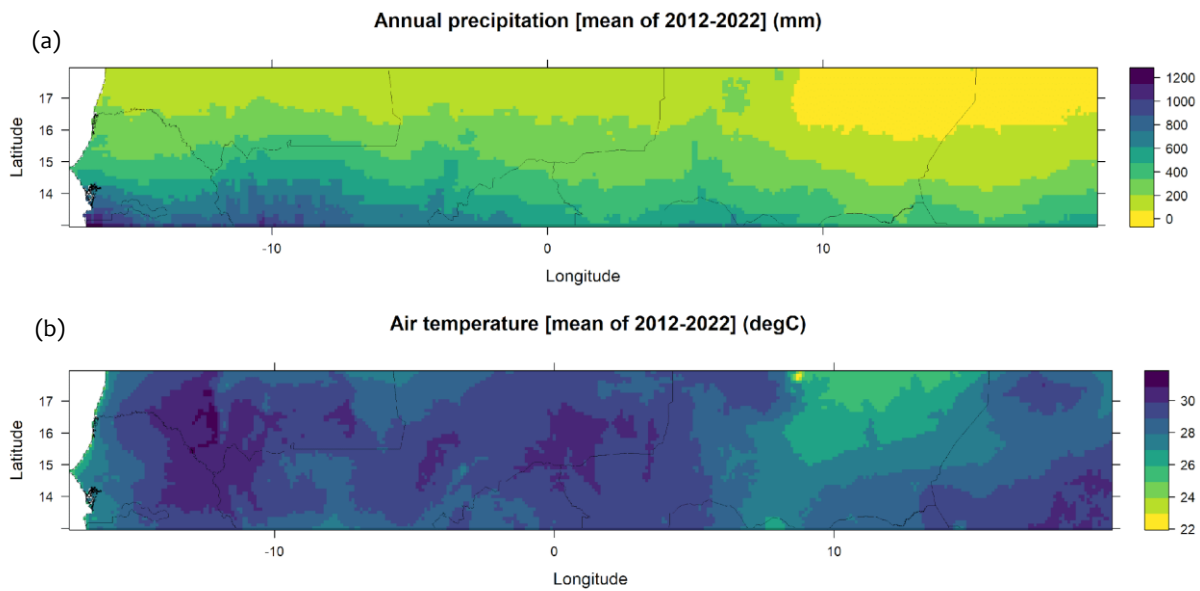


Figure A1: Spatial distribution of silvopastoral areas in the Sahel. (Details on how the percentage of silvopastoral area pixels within the simulation grid cells were computed are provided in Methodology, Session 2.4)



595

Figure A2: Spatial distribution of precipitation and air temperature (mean over 2012-2022).

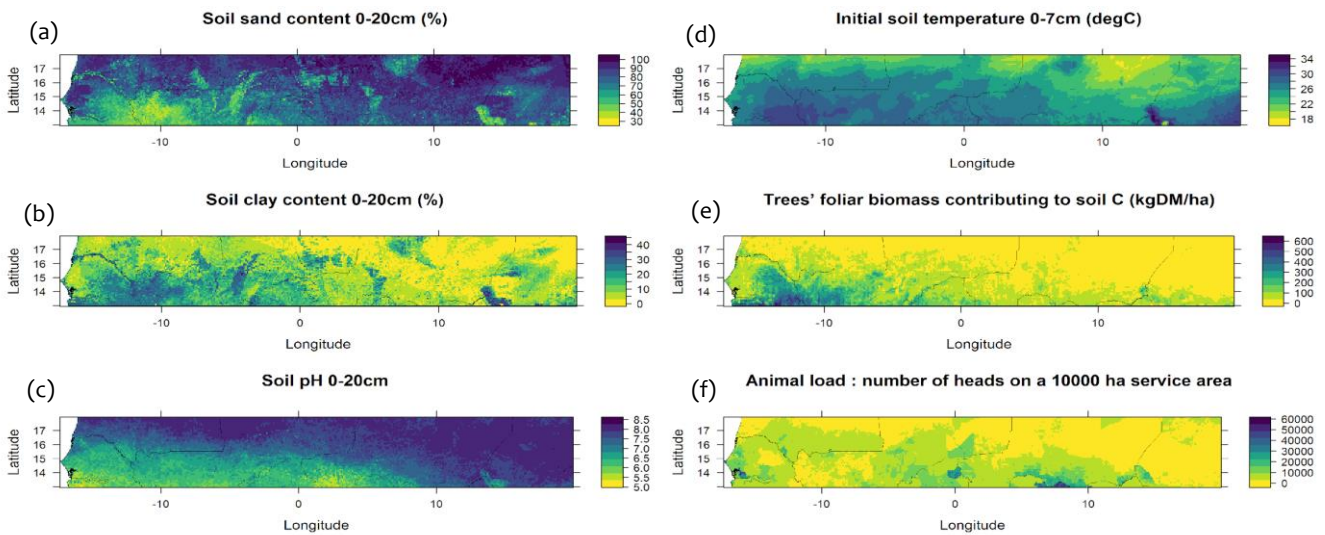


Figure A3: Spatial distribution of soil properties, trees' foliar biomass and livestock

600

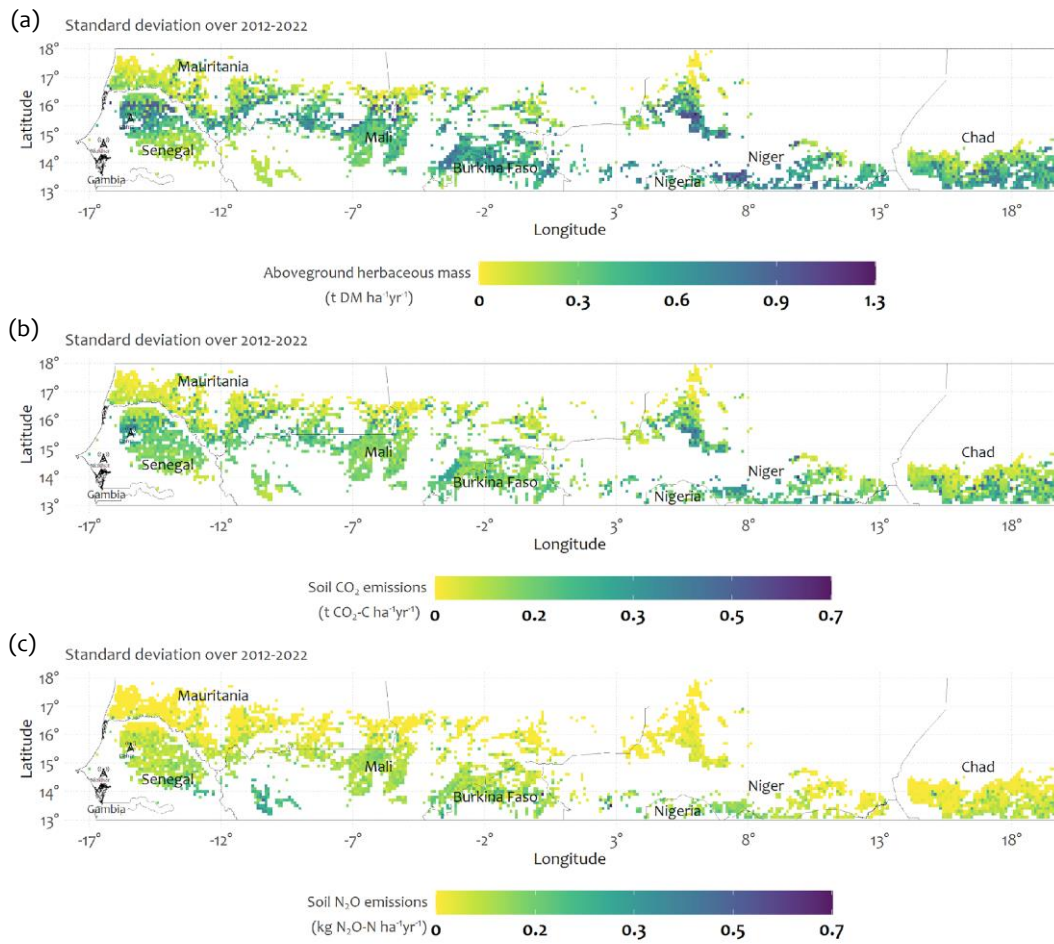
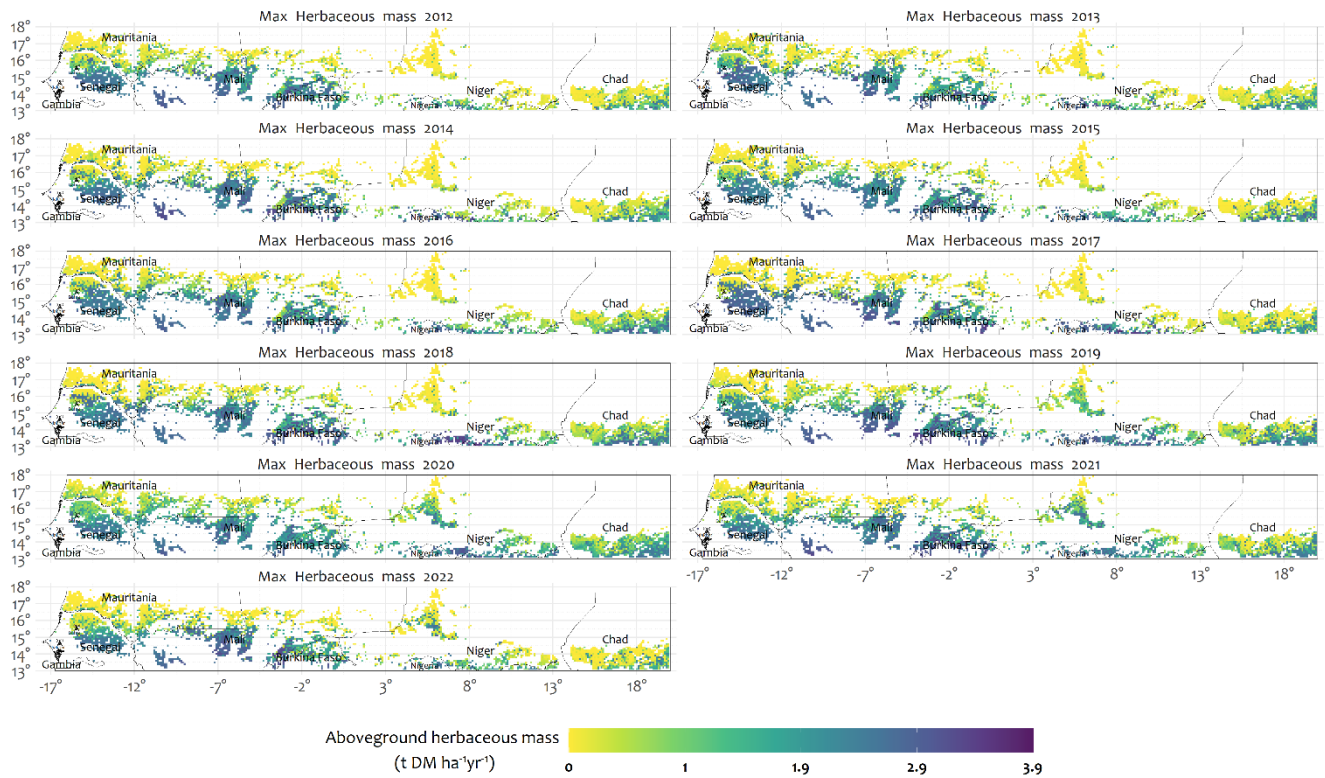
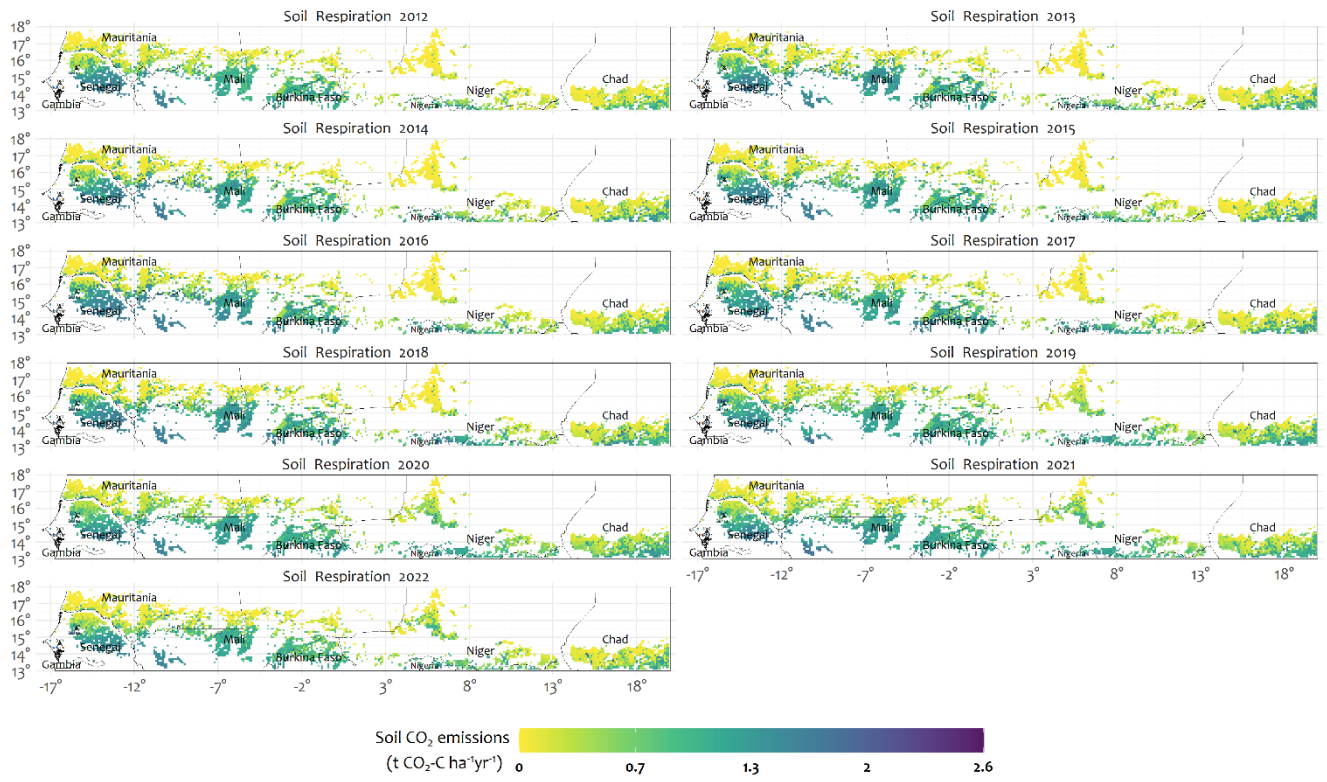


Figure A4: Standard deviations of the spatial distribution of (a) herbaceous biomass, (b) soil CO₂ and (c) soil N₂O emissions in Sahelian SPSs (over 2012-2022). Only pixels dominated by SPSs (>80%) are displayed



605

Figure A5: Annual spatial distribution of herbaceous biomass in Sahelian SPSs (2012-2022). Only pixels dominated by SPSs (>80%) are displayed



610 **Figure A6: Annual spatial distribution of soil CO₂ emissions in Sahelian SPSs (2012-2022). Only pixels dominated by SPSs (>80%) are displayed**

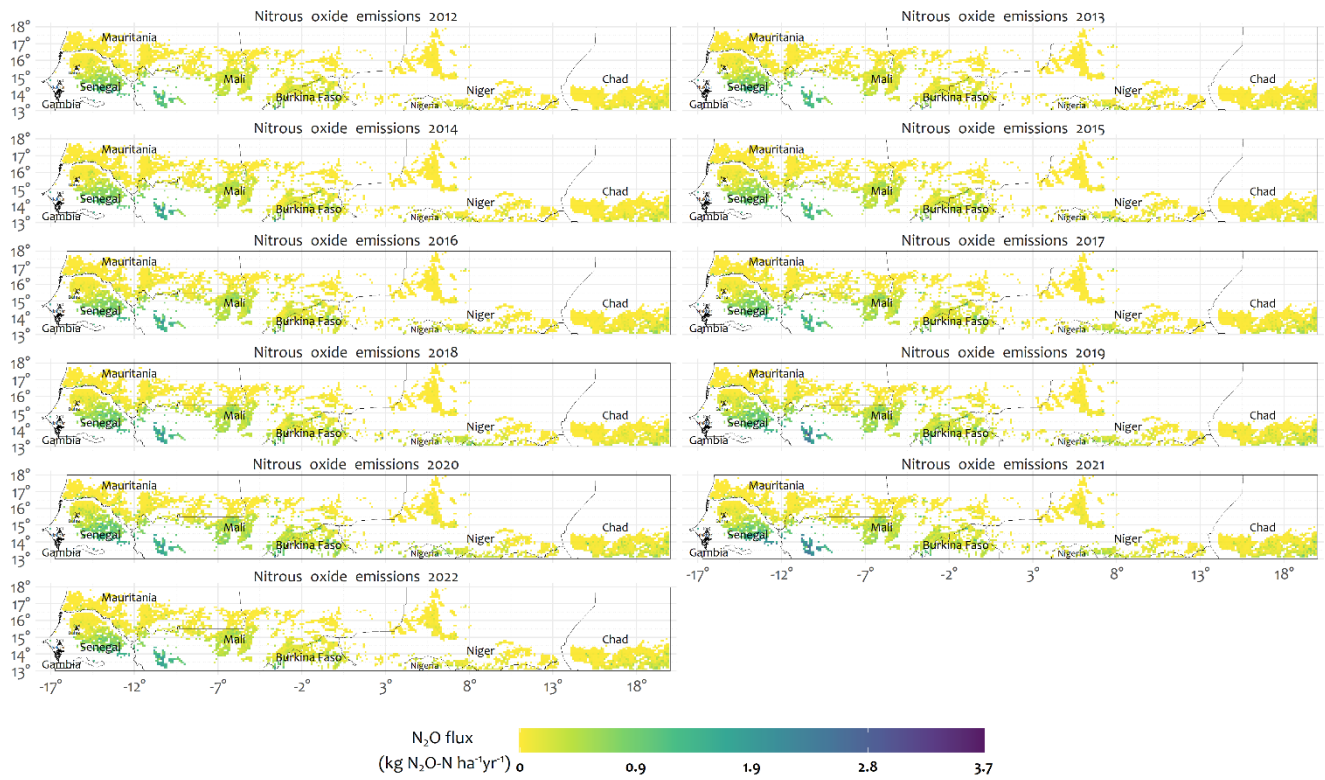


Figure A7: Annual spatial distribution of soil N₂O emissions in Sahelian SPSs (2012-2022). Only pixels dominated by SPSs (>80%) are displayed

615

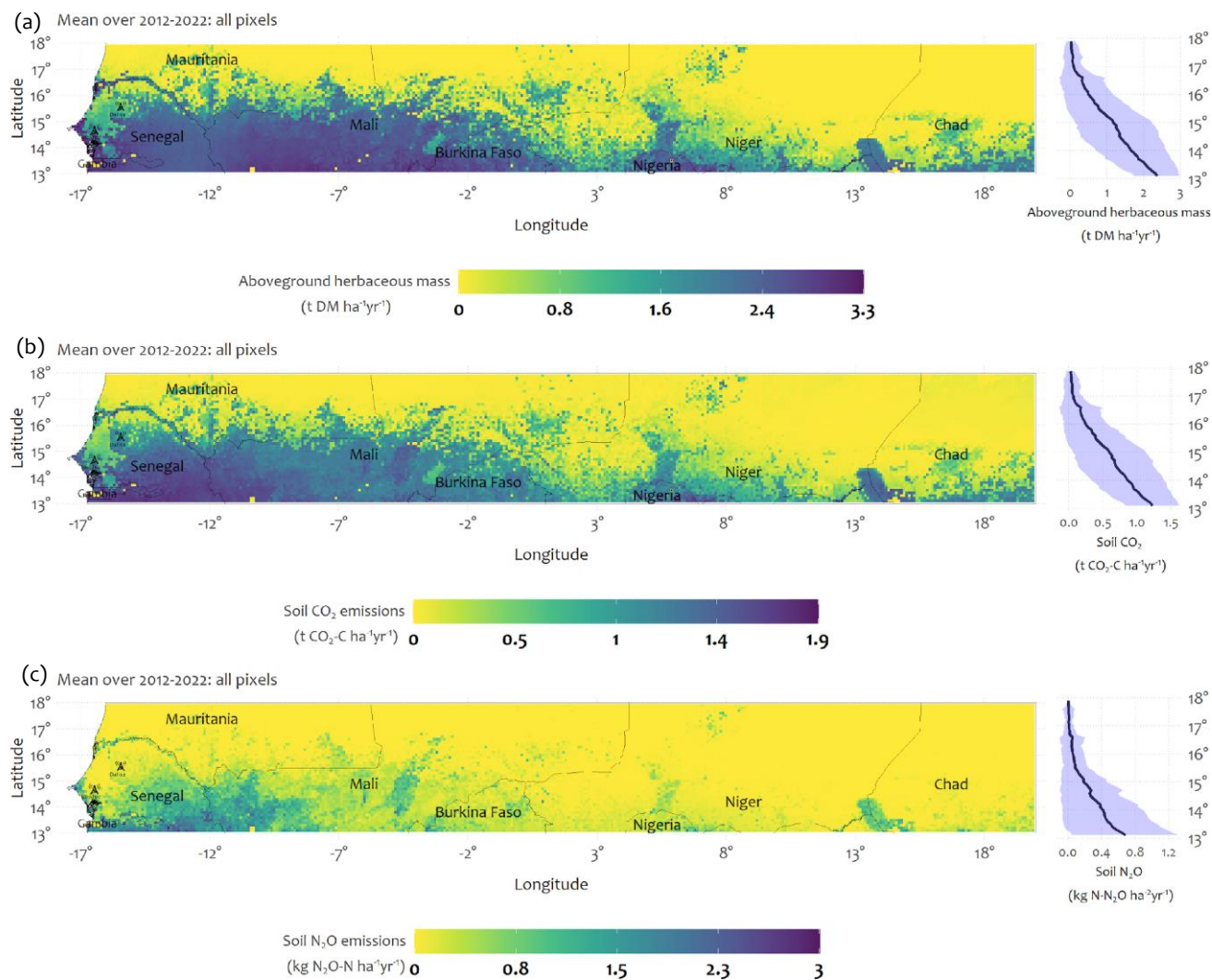
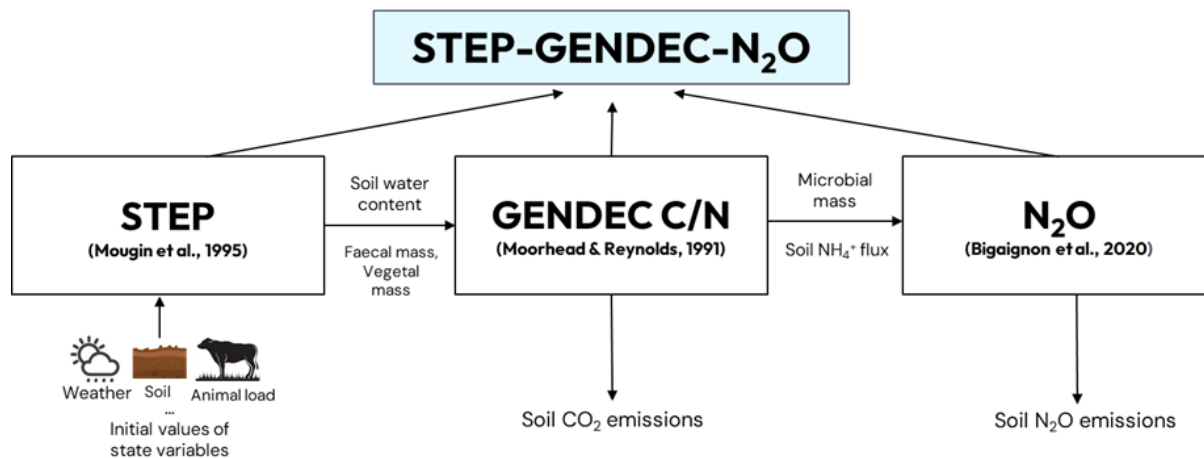


Figure A8: Regional distribution of simulated (a) herbaceous biomass, (b) soil CO₂ and (c) soil N₂O emissions in Sahelian SPSS (annual mean over 2012-2022). All pixels are displayed. The right panel shows (a) herbaceous biomass, (b) soil CO₂ and (c) soil N₂O emissions along a latitudinal gradient of 0.1°, while the shaded area indicates the standard deviation.



620

Figure A9: Summary figure showing the connection between the models STEP, GENDEC, and the N₂O module.

Code availability. The 2D STEP-GENDEC-N₂O model is available on Zenodo at <https://doi.org/10.5281/zenodo.7866671>. The "rstep" R package (Agbohessou, 2022), developed to automate workflows for 1D and 2D STEP-GENDEC-N₂O simulations, has been archived on Zenodo at: <https://doi.org/10.5281/zenodo.7994028>.

625

Author contribution. YA, CD, MG, EM, and OR conceived and designed the study. EM, CD, MG, and YA developed the 2D STEP-GENDEC-N₂O model code and YA performed the simulations. YA prepared the manuscript with contributions from all co-authors.

Competing interests. The authors declare that they have no conflict of interest.

630

Funding. This work was supported by the “Carbon sequestration and greenhouse gas emissions in (agro) silvopastoral ecosystems in the Sahelian CILSS states” (CaSSECS) project (FOOD/2019/410-169), which received funding from the European Union under the “Development of Smart Innovation through Research in Agriculture” (DeSIRA) Initiative. Additionally, this research received financial support from the “Intergrated Nitrogen Studies in Africa” (INSA) project, which is supported by the European Union’s Horizon 2020 Research and Innovation programme under the Marie Skłodowska-Curie Actions (RISE MSCA) Grant Agreement n° 871944.

635

Mention. This document has been produced with the assistance of the European Union. Its content is the sole responsibility of the authors and can in no way be taken to reflect the position of the European Union.

Acknowledgments. The authors gratefully acknowledge the use of the Nuwa high-performance computing cluster from Toulouse-France, which provided the essential computing resources that facilitated the research presented in this paper.

Additionally, the authors wish to express their appreciation to Anne Mottet for sharing relevant literature on land cover products.

640

References

Agbohessou, Y.: rstep: a workflow for STEP-GENDEC-CN model under R, , <https://doi.org/10.5281/zenodo.7994028>, 2022.

645

Agbohessou, Y., Delon, C., Mougin, E., Grippa, M., Tagesson, T., Diedhiou, M., Ba, S., Ngom, D., Vezy, R., Ndiaye, O., Assouma, M. H., Diawara, M., and Roupsard, O.: To what extent are greenhouse-gas emissions offset by trees in a Sahelian silvopastoral system?, *Agricultural and Forest Meteorology*, 343, 109780, <https://doi.org/10.1016/j.agrformet.2023.109780>, 2023.

Assouma, M. H., Serça, D., Guérin, F., Blanfort, V., Lecomte, P., Touré, I., Ickowicz, A., Manlay, R. J., Bernoux, M., and Vayssières, J.: Livestock induces strong spatial heterogeneity of soil CO₂, N₂O and CH₄ emissions within a semi-arid silvopastoral landscape in West Africa, *J. Arid Land*, 9, 210–221, <https://doi.org/10.1007/s40333-017-0001-y>, 2017.

650

Aulakh, M. S., Doran, J. W., Walters, D. T., and Power, J. F.: Legume residue and soil water effects on denitrification in soils of different textures, *Soil Biology and Biochemistry*, 23, 1161–1167, 1991.

Aulakh, M. S., Doran, J. W., and Mosier, A. R.: Soil denitrification—significance, measurement, and effects of management, in: *Advances in soil science*, Springer, 1–57, 1992.

655

Bajracharya, R. M., Lal, R., and Kimble, J. M.: Diurnal and seasonal CO₂–C flux from soil as related to erosion phases in central Ohio, *Soil Science Society of America Journal*, 64, 286–293, 2000.

Ballabio, C., Panagos, P., and Monatanarella, L.: Mapping topsoil physical properties at European scale using the LUCAS database, *Geoderma*, 261, 110–123, <https://doi.org/10.1016/j.geoderma.2015.07.006>, 2016.

Barnard, R. L., Blazewicz, S. J., and Firestone, M. K.: Rewetting of soil: Revisiting the origin of soil CO₂ emissions, *Soil Biology and Biochemistry*, 147, 107819, <https://doi.org/10.1016/j.soilbio.2020.107819>, 2020.

660

Bernard, C. and Fillol, E.: PRODUCTION DE BIOMASSE EN 2020 ANALYSES ET PERSPECTIVES POUR 202, 10, 2020.

Bernard, C. and Fillol, E.: PRODUCTION DE BIOMASSE EN 2021 ANALYSES ET PERSPECTIVES POUR 2022, 10, 2021.

Biasutti, M.: Rainfall trends in the African Sahel: Characteristics, processes, and causes, *WIREs Climate Change*, 10, e591, <https://doi.org/10.1002/wcc.591>, 2019.

665

Bigaignon, L., Delon, C., Ndiaye, O., Galy-Lacaux, C., Serça, D., Guérin, F., Tallec, T., Merbold, L., Tagesson, T., Fensholt, R., André, S., and Galliau, S.: Understanding N₂O Emissions in African Ecosystems: Assessments from a Semi-Arid Savanna Grassland in Senegal and Sub-Tropical Agricultural Fields in Kenya, 26, 2020.

Birch, H. F.: The effect of soil drying on humus decomposition and nitrogen availability, *Plant and soil*, 10, 9–31, 1958.

670

Bloch-Johnson, J., Rugenstein, M., Stolpe, M. B., Rohrschneider, T., Zheng, Y., and Gregory, J. M.: Climate Sensitivity Increases Under Higher CO₂ Levels Due to Feedback Temperature Dependence, *Geophysical Research Letters*, 48, e2020GL089074, <https://doi.org/10.1029/2020GL089074>, 2021.

- Bond-Lamberty, B. and Thomson, A.: A global database of soil respiration data, *Biogeosciences*, 7, 1915–1926, <https://doi.org/10.5194/bg-7-1915-2010>, 2010.
- 675 Boogaard, H., Schubert, De Wit, A., Lazebnik, J., Hutjes, R., and Van der Grijn, G.: Agrometeorological indicators from 1979 to present derived from reanalysis, version 1.0. Copernicus Climate Change Service (C3S) Climate Data Store (CDS), (Accessed on 18-June-2022), <https://doi.org/10.24381/CDS.6C68C9BB>, 2020.
- Breiman, L.: Random Forests, *Machine Learning*, 45, 5–32, <https://doi.org/10.1023/A:1010933404324>, 2001.
- Breiman, L., Friedman, J., Olshen, R., and Stone, C.: *Classification and regression trees*—crc press, Boca Raton, Florida, 1984.
- Brown, D. and de Sousa, K.: ag5Tools: Toolbox for Downloading and Extracting Copernicus AgERA5 Data, 2022.
- 680 Brümmer, C., Papen, H., Wassmann, R., and Brüggemann, N.: Termite mounds as hot spots of nitrous oxide emissions in South-Sudanian savanna of Burkina Faso (West Africa), *Geophys. Res. Lett.*, 36, L09814, <https://doi.org/10.1029/2009GL037351>, 2009.
- 685 Butterbach-Bahl, K., Baggs, E. M., Dannenmann, M., Kiese, R., and Zechmeister-Boltenstern, S.: Nitrous oxide emissions from soils: how well do we understand the processes and their controls?, *Philosophical Transactions of the Royal Society B: Biological Sciences*, 368, 20130122, <https://doi.org/10.1098/rstb.2013.0122>, 2013.
- Butterbach-Bahl, K., Gettel, G., Kiese, R., Fuchs, K., Werner, C., Rahimi, J., Barthel, M., and Merbold, L.: Livestock enclosures in drylands of Sub-Saharan Africa are overlooked hotspots of N₂O emissions, *Nat Commun*, 11, 4644, <https://doi.org/10.1038/s41467-020-18359-y>, 2020.
- 690 Cao, P., Lu, C., and Yu, Z.: Historical nitrogen fertilizer use in agricultural ecosystems of the contiguous United States during 1850–2015: application rate, timing, and fertilizer types, *Earth System Science Data*, 10, 969–984, 2018.
- Chagnaud, G., Panthou, G., Vischel, T., and Lebel, T.: A synthetic view of rainfall intensification in the West African Sahel, *Environ. Res. Lett.*, 17, 044005, <https://doi.org/10.1088/1748-9326/ac4a9c>, 2022.
- Chang, J., Ciais, P., Viovy, N., Vuichard, N., Sultan, B., and Soussana, J.-F.: The greenhouse gas balance of European grasslands, *Global Change Biology*, 21, 3748–3761, <https://doi.org/10.1111/gcb.12998>, 2015.
- 695 Chevallier, T., Hmaid, K., Kouakoua, E., Bernoux, M., Gallali, T., Toucet, J., Jolivet, C., Deleporte, P., and Barthès, B. G.: Physical protection of soil carbon in macroaggregates does not reduce the temperature dependence of soil CO₂ emissions, *Journal of Plant Nutrition and Soil Science*, 178, 592–600, 2015.
- 700 Cuhel, J., Šimek, M., Laughlin, R. J., Bru, D., Chèneby, D., Watson, C. J., and Philippot, L.: Insights into the effect of soil pH on N₂O and N₂ emissions and denitrifier community size and activity, *Applied and environmental microbiology*, 76, 1870–1878, 2010.
- Dai, A., Lamb, P. J., Trenberth, K. E., Hulme, M., Jones, P. D., and Xie, P.: The recent Sahel drought is real, *International Journal of Climatology: A Journal of the Royal Meteorological Society*, 24, 1323–1331, 2004.
- Dangal, S. R. S., Tian, H., Pan, S., Zhang, L., and Xu, R.: Greenhouse gas balance in global pasturelands and rangelands, *Environ. Res. Lett.*, 15, 104006, <https://doi.org/10.1088/1748-9326/abaa79>, 2020.
- 705 Davidson, E. A.: The contribution of manure and fertilizer nitrogen to atmospheric nitrous oxide since 1860, *Nature Geoscience*, 2, 659–662, <https://doi.org/10.1038/ngeo608>, 2009.

- Davidson, E. A. and Kanter, D.: Inventories and scenarios of nitrous oxide emissions, *Environ. Res. Lett.*, 9, 105012, <https://doi.org/10.1088/1748-9326/9/10/105012>, 2014.
- 710 Davidson, E. A. and Swank, W. T.: Environmental parameters regulating gaseous nitrogen losses from two forested ecosystems via nitrification and denitrification, *Applied and Environmental Microbiology*, 52, 1287–1292, 1986.
- Davidson, E. A. and Verchot, L. V.: Testing the hole-in-the-pipe model of nitric and nitrous oxide emissions from soils using the TRAGNET database, *Global Biogeochemical Cycles*, 14, 1035–1043, 2000.
- 715 Delon, C., Mougin, E., Serça, D., Grippa, M., Hiernaux, P., Diawara, M., Galy-Lacaux, C., and Kergoat, L.: Modelling the effect of soil moisture and organic matter degradation on biogenic NO emissions from soils in Sahel rangeland (Mali), *Biogeosciences*, 12, 3253–3272, <https://doi.org/10.5194/bg-12-3253-2015>, 2015.
- Delon, C., Galy-Lacaux, C., Serça, D., Loubet, B., Camara, N., Gardrat, E., Saneh, I., Fensholt, R., Tagesson, T., Le Dantec, V., Sambou, B., Diop, C., and Mougin, E.: Soil and vegetation-atmosphere exchange of NO, NH₃, and N₂O from field measurements in a semi arid grazed ecosystem in Senegal, *Atmospheric Environment*, 156, 36–51, <https://doi.org/10.1016/j.atmosenv.2017.02.024>, 2017.
- 720 Delon, C., Galy-Lacaux, C., Serça, D., Personne, E., Mougin, E., Adon, M., Le Dantec, V., Loubet, B., Fensholt, R., and Tagesson, T.: Modelling land–atmosphere daily exchanges of NO, NH₃, and CO₂ in a semi-arid grazed ecosystem in Senegal, *Biogeosciences*, 16, 2049–2077, <https://doi.org/10.5194/bg-16-2049-2019>, 2019.
- Dezfuli, A. K., Ichoku, C. M., Huffman, G. J., Mohr, K. I., Selker, J. S., Van De Giesen, N., Hochreutener, R., and Annor, F. O.: Validation of IMERG precipitation in Africa, *Journal of Hydrometeorology*, 18, 2817–2825, 2017.
- 725 Echeverry-Galvis, M. A., Peterson, J. K., and Sulo-Caceres, R.: The social network: Tree structure determines nest placement in kenyan weaverbird colonies, *PloS one*, 9, e88761, 2014.
- Efron, B. and Tibshirani, R.: Bootstrap methods for standard errors, confidence intervals, and other measures of statistical accuracy, *Statistical science*, 54–75, 1986.
- 730 Elberling, B., Touré, A., and Rasmussen, K.: Changes in soil organic matter following groundnut–millet cropping at three locations in semi-arid Senegal, West Africa, *Agriculture, ecosystems & environment*, 96, 37–47, 2003a.
- Elberling, B., Fensholt, R., Larsen, L., Petersen, A. S., and Sandholt, I.: Water content and land use history controlling soil CO₂ respiration and carbon stock in savanna soil and groundnut fields in semi-arid Senegal, *Geografisk Tidsskrift-Danish Journal of Geography*, 103, 47–56, 2003b.
- 735 Fan, Z., Neff, J. C., and Hanan, N. P.: Modeling pulsed soil respiration in an African savanna ecosystem, *Agricultural and Forest Meteorology*, 200, 282–292, 2015.
- FAOSTAT: Crops and livestock products, 2024.
- 740 Galle, S., Grippa, M., Peugeot, C., Moussa, I. B., Cappelaere, B., Demarty, J., Mougin, E., Panthou, G., Adjomayi, P., Agbossou, E. k., Ba, A., Boucher, M., Cohard, J.-M., Descloitres, M., Descroix, L., Diawara, M., Dossou, M., Favreau, G., Gangneron, F., Gosset, M., Hector, B., Hiernaux, P., Issoufou, B.-A., Kergoat, L., Lawin, E., Lebel, T., Legchenko, A., Abdou, M. M., Malam-Issa, O., Mamadou, O., Nazoumou, Y., Pellarin, T., Quantin, G., Sambou, B., Seghieri, J., Séguis, L., Vandervaere, J.-P., Viscel, T., Vouillamoz, J.-M., Zannou, A., Afouda, S., Alhassane, A., Arjounin, M., Barral, H., Biron, R., Cazenave, F., Chaffard, V., Chazarin, J.-P., Guyard, H., Koné, A., Mainassara, I., Mamane, A., Oi, M., Ouani, T., Soumaguel, N., Wubda, M., Ago, E. e., Alle, I. c., Allies, A., Arpin-Pont, F., Awessou, B., Cassé, C., Charvet, G., Dardel, C.,

- 745 Depeyre, A., Diallo, F. b., Do, T., Fatras, C., Frappart, F., Gal, L., Gascon, T., Gibon, F., Guiro, I., Ingatan, A., Kempf, J., Kotchoni, D. o. v., Lawson, F. m. a., Leauthaud, C., Louvet, S., Mason, E., Nguyen, C. c., Perrimond, B., Pierre, C., Richard, A., Robert, E., Román-Cascón, C., Velluet, C., and Wilcox, C.: AMMA-CATCH, a Critical Zone Observatory in West Africa Monitoring a Region in Transition, *Vadose Zone Journal*, 17, 180062, <https://doi.org/10.2136/vzj2018.03.0062>, 2018.
- Ghattas, B.: Agrégation d'arbres de classification, *Revue de statistique appliquee*, 48, 85–98, 2000.
- 750 Gilbert, M., Nicolas, G., Cinardi, G., Van Boeckel, T. P., Vanwambeke, S. O., Wint, G. R. W., and Robinson, T. P.: Global distribution data for cattle, buffaloes, horses, sheep, goats, pigs, chickens and ducks in 2010, *Sci Data*, 5, 180227, <https://doi.org/10.1038/sdata.2018.227>, 2018.
- Gleixner, S., Demissie, T., and Diro, G. T.: Did ERA5 improve temperature and precipitation reanalysis over East Africa?, *Atmosphere*, 11, 996, 2020.
- 755 Grippa, M., Kergoat, L., Boone, A., Peugeot, C., Demarty, J., Cappelaere, B., Gal, L., Hiernaux, P., Mougin, E., Ducharne, A., Dutra, E., Anderson, M., Hain, C., and ALMIP2 Working Group: Modeling Surface Runoff and Water Fluxes over Contrasted Soils in the Pastoral Sahel: Evaluation of the ALMIP2 Land Surface Models over the Gourma Region in Mali, *Journal of Hydrometeorology*, 18, 1847–1866, <https://doi.org/10.1175/JHM-D-16-0170.1>, 2017.
- 760 Guichard, F., Kergoat, L., Hourdin, F., Léauthaud, C., Barbier, J., Mougin, É., and Diarra, B.: Chapter 1. Climate warming observed in the Sahel since 1950, in: *Rural societies in the face of climatic and environmental changes in West Africa*, edited by: Lalou, R., Oumarou, A., Sanni, M. A., Sultan, B., and Arame Soumaré, M., IRD Éditions, Marseille, 23–41, <https://doi.org/10.4000/books.irdeditions.12319>, 2020.
- 765 Hengl, T., Miller, M. A. E., Križan, J., Shepherd, K. D., Sila, A., Kilibarda, M., Antonijević, O., Glušica, L., Dobermann, A., Haefele, S. M., McGrath, S. P., Acquah, G. E., Collinson, J., Parente, L., Sheykhmousa, M., Saito, K., Johnson, J.-M., Chamberlin, J., Silatsa, F. B. T., Yemefack, M., Wendt, J., MacMillan, R. A., Wheeler, I., and Crouch, J.: African soil properties and nutrients mapped at 30 m spatial resolution using two-scale ensemble machine learning, *Sci Rep*, 11, 6130, <https://doi.org/10.1038/s41598-021-85639-y>, 2021.
- Hergoualc'h, K., Akiyama, H., Bernoux, M., Chirinda, N., Prado, A. del, Kasimir, Å., MacDonald, J. D., Ogle, S. M., Regina, K., and Weerden, T. J. van der: N2O emissions from managed soils, and CO2 emissions from lime and urea application, 2019.
- 770 Herrero, M., Havlík, P., Valin, H., Notenbaert, A., Rufino, M. C., Thornton, P. K., Blümmel, M., Weiss, F., Grace, D., and Obersteiner, M.: Biomass use, production, feed efficiencies, and greenhouse gas emissions from global livestock systems, *Proceedings of the National Academy of Sciences*, 110, 20888–20893, <https://doi.org/10.1073/pnas.1308149110>, 2013a.
- Herrero, M., Grace, D., Njuki, J., Johnson, N., Enahoro, D., Silvestri, S., and Rufino, M. C.: The roles of livestock in developing countries, *Animal*, 7, 3–18, <https://doi.org/10.1017/S1751731112001954>, 2013b.
- 775 Hiernaux, P., Diarra, L., Trichon, V., Mougin, E., Soumaguel, N., and Baup, F.: Woody plant population dynamics in response to climate changes from 1984 to 2006 in Sahel (Gourma, Mali), *Journal of Hydrology*, 375, 103–113, <https://doi.org/10.1016/j.jhydrol.2009.01.043>, 2009.
- Hiernaux, P., Issoufou, H. B.-A., Igel, C., Kariryaa, A., Kourouma, M., Chave, J., Mougin, E., and Savadogo, P.: Allometric equations to estimate the dry mass of Sahel woody plants mapped with very-high resolution satellite imagery, *Forest Ecology and Management*, 529, 120653, <https://doi.org/10.1016/j.foreco.2022.120653>, 2023.

- 780 Huffman, G. J., Stocker, E. F., Bolvin, D. T., Nelkin, E. J., and Tan, J.: GPM IMERG Final Precipitation L3 1 day 0.1 degree x 0.1 degree V06, Edited by Andrey Savtchenko, Greenbelt, MD, Goddard Earth Sciences Data and Information Services Center (GES DISC), doi. org/10.5067/GPM/IMERG DF/DAY/06, 2019.
- IPCC: 2006 IPCC Guidelines for National Greenhouse Gas Inventories, 2006.
- 785 Jarlan, L., Mazzega, P., Mougin, E., Lavenu, F., Marty, G., Frison, P. L., and Hiernaux, P.: Mapping of Sahelian vegetation parameters from ERS scatterometer data with an evolution strategies algorithm, *Remote Sensing of Environment*, 87, 72–84, 2003.
- Jarlan, L., Mougin, E., Mazzega, P., Schoenauer, M., Tracol, Y., and Hiernaux, P.: Using coarse remote sensing radar observations to control the trajectory of a simple Sahelian land surface model, *Remote Sensing of Environment*, 94, 269–285, 2005.
- 790 Jarlan, L., Mangiarotti, S., Mougin, E., Mazzega, P., Hiernaux, P., and Le Dantec, V.: Assimilation of SPOT/VEGETATION NDVI data into a sahelian vegetation dynamics model, *Remote Sensing of Environment*, 112, 1381–1394, 2008.
- Jarvis, P., Rey, A., Petsikos, C., Wingate, L., Rayment, M., Pereira, J., Banza, J., David, J., Miglietta, F., and Borghetti, M.: Drying and wetting of Mediterranean soils stimulates decomposition and carbon dioxide emission: the “Birch effect,” *Tree physiology*, 27, 929–940, 2007.
- 795 Kammen, D. M. and Marino, B. D.: On the origin and magnitude of pre-industrial anthropogenic CO₂ and CH₄ emissions, *Chemosphere*, 26, 69–86, [https://doi.org/10.1016/0045-6535\(93\)90413-Y](https://doi.org/10.1016/0045-6535(93)90413-Y), 1993.
- Karhu, K., Dannenmann, M., Kitzler, B., Díaz-Pinés, E., Tejedor, J., Ramírez, D. A., Parra, A., De Dios, V. R., Moreno, J. M., and Rubio, A.: Fire increases the risk of higher soil N₂O emissions from Mediterranean *Macchia* ecosystems, *Soil Biology and Biochemistry*, 82, 44–51, 2015.
- 800 Khalil, K.: Emissions de N₂O par nitrification et dénitrification à l'échelle de la motte de sol: effet de la structure du sol, de l'aération et des activités microbiennes, Université Paris 6, 2015.
- Lambert, M.-J., Bana, Z. S., and Oualbiogo, H. V.: PRODUCTION DE BIOMASSE AU SAHEL EN 2019, 8, 2019.
- Latham, J., Cumani, R., Rosati, I., and Bloise, M.: Global land cover share (GLC-SHARE) database beta-release version 1.0-2014, FAO: Rome, Italy, 29, 2014.
- 805 Lavers, D. A., Simmons, A., Vamborg, F., and Rodwell, M. J.: An evaluation of ERA5 precipitation for climate monitoring, *Quart J Royal Meteor Soc*, 148, 3152–3165, <https://doi.org/10.1002/qj.4351>, 2022.
- Le Houerou, H. N.: Indigenous shrubs and trees in the silvopastoral systems of Africa, *Agroforestry*, 139, 1987.
- Le Houérou, H. N.: Classification écoclimatique des zones arides (sl) de l'Afrique du Nord, *Ecologia mediterranea*, 15, 95–144, 1989.
- 810 Leahy, P.: Managed grasslands: A greenhouse gas sink or source?, *Geophys. Res. Lett.*, 31, L20507, <https://doi.org/10.1029/2004GL021161>, 2004.
- Li, C., Aber, J., Stange, F., Butterbach-Bahl, K., and Papen, H.: A process-oriented model of N₂O and NO emissions from forest soils: 1. Model development, *Journal of Geophysical Research: Atmospheres*, 105, 4369–4384, 2000.

- Liaw, A. and Wiener, M.: Classification and regression by randomForest, *R news*, 2, 18–22, 2002.
- 815 Liu, Y.: Modeling the emissions of nitrous oxide (N₂O) and methane (CH₄) from the terrestrial biosphere to the atmosphere, Massachusetts Institute of Technology, 1996.
- Liu, Y., Wu, X., Wu, T., Zhao, L., Li, R., Li, W., Hu, G., Zou, D., Ni, J., Du, Y., Wang, M., Li, Z., Wei, X., and Yan, X.: Soil Texture and Its Relationship with Environmental Factors on the Qinghai–Tibet Plateau, *Remote Sensing*, 14, 3797, <https://doi.org/10.3390/rs14153797>, 2022.
- 820 Lloyd, J. and Taylor, J. A.: On the Temperature Dependence of Soil Respiration, *Functional Ecology*, 8, 315–323, <https://doi.org/10.2307/2389824>, 1994.
- Ma, S., Baldocchi, D. D., Hatala, J. A., Detto, M., and Yuste, J. C.: Are rain-induced ecosystem respiration pulses enhanced by legacies of antecedent photodegradation in semi-arid environments?, *Agricultural and Forest Meteorology*, 154, 203–213, 2012.
- 825 Maavara, T., Lauerwald, R., Laruelle, G. G., Akbarzadeh, Z., Bouskill, N. J., Van Cappellen, P., and Regnier, P.: Nitrous oxide emissions from inland waters: Are IPCC estimates too high?, *Global change biology*, 25, 473–488, 2019.
- Macfadyen, A.: Soil metabolism in relation to ecosystem energy flow and to primary and secondary production., in: “Methods of Study in Soil Ecology” Proc. UNESCO/IBP Symp. Paris 1967., 167–172, 1970.
- 830 Maranan, M., Fink, A. H., Knippertz, P., Amekudzi, L. K., Atiah, W. A., and Stengel, M.: A process-based validation of GPM IMERG and its sources using a mesoscale rain gauge network in the West African forest zone, *Journal of Hydrometeorology*, 21, 729–749, 2020.
- Miller, M. A., Shepherd, K. D., Kisitu, B., and Collinson, J.: iSDAsoil: The first continent-scale soil property map at 30 m resolution provides a soil information revolution for Africa, *PLoS Biology*, 19, e3001441, 2021.
- Monteith, J. L.: Solar radiation and productivity in tropical ecosystems, *Journal of applied ecology*, 9, 747–766, 1972.
- 835 Moorhead, D. L. and Reynolds, J. F.: A general model of litter decomposition in the northern Chihuahuan Desert, *Ecological Modelling*, 56, 197–219, [https://doi.org/10.1016/0304-3800\(91\)90200-K](https://doi.org/10.1016/0304-3800(91)90200-K), 1991.
- Mougin, E., Lo Seen, D., Rambal, S., Gaston, A., and Hiernaux, P.: A regional Sahelian grassland model to be coupled with multispectral satellite data. I: Model description and validation, *Remote Sensing of Environment*, 52, 181–193, [https://doi.org/10.1016/0034-4257\(94\)00126-8](https://doi.org/10.1016/0034-4257(94)00126-8), 1995.
- 840 Muñoz Sabater, J.: ERA5-Land hourly data from 1981 to present. Copernicus Climate Change Service (C3S) Climate Data Store (CDS), (Accessed on < 18-June-2022 >), <https://doi.org/10.24381/CDS.E2161BAC>, 2019.
- Muñoz-Sabater, J., Dutra, E., Agustí-Panareda, A., Albergel, C., Arduini, G., Balsamo, G., Boussetta, S., Choulga, M., Harrigan, S., Hersbach, H., Martens, B., Miralles, D. G., Piles, M., Rodríguez-Fernández, N. J., Zsoter, E., Buontempo, C., and Thépaut, J.-N.: ERA5-Land: a state-of-the-art global reanalysis dataset for land applications, *Earth System Science Data*, 13, 4349–4383, <https://doi.org/10.5194/essd-13-4349-2021>, 2021.
- Nicholson, S. E.: Climate and climatic variability of rainfall over eastern Africa, *Rev. Geophys.*, 55, 590–635, <https://doi.org/10.1002/2016RG000544>, 2017.

- Oertel, C., Matschullat, J., Zurba, K., Zimmermann, F., and Erasmí, S.: Greenhouse gas emissions from soils—A review, *Geochemistry*, 76, 327–352, <https://doi.org/10.1016/j.chemer.2016.04.002>, 2016.
- 850 Parmesan, C., Morecroft, M., Trisurat, Y., Adrian, R., Anshari, G., Arneth, A., Gao, Q., Gonzalez, P., Harris, R., Price, J., Stevens, N., Talukdarr, G., Strutz, S., Ackerly, D., Anderson, E., Boyd, P., Birkmann, J., Bremerich, V., Brotons, L., and Young, K.: IPCC AR6 WGII Chapter 2 - Terrestrial and Freshwater Ecosystems and Their Services, in: *Climate Change 2022: Impacts, Adaptation, and Vulnerability. Contribution of Working Group II to the Sixth Assessment Report of the Intergovernmental Panel on Climate Change* [H.-O. Pörtner, D.C. Roberts, M. Tignor, E.S. Poloczanska, K. Mintenbeck, A. 855 Alegría, M. Craig, S. Langsdorf, S. Löschke, V. Möller, A. Okem, B. Rama (eds.)], Cambridge, UK and New York, NY, USA, 197–377, <https://doi.org/10.1017/9781009325844.004>, 2022.
- Parton, W. J., Holland, E. A., Del Grosso, S. J., Hartman, M. D., Martin, R. E., Mosier, A. R., Ojima, D. S., and Schimel, D. S.: Generalized model for NO_x and N₂O emissions from soils, *Journal of Geophysical Research: Atmospheres*, 106, 17403–17419, 2001.
- 860 Philibert, A., Loyce, C., and Makowski, D.: Prediction of N₂O emission from local information with Random Forest, *Environmental Pollution*, 177, 156–163, <https://doi.org/10.1016/j.envpol.2013.02.019>, 2013.
- Pierre, C., Bergametti, G., Marticorena, B., Mougin, E., Lebel, T., and Ali, A.: Pluriannual comparisons of satellite-based rainfall products over the Sahelian belt for seasonal vegetation modeling, *J. Geophys. Res.*, 116, D18201, <https://doi.org/10.1029/2011JD016115>, 2011.
- 865 Pierre, C., Grippa, M., Mougin, E., Guichard, F., and Kergoat, L.: Changes in Sahelian annual vegetation growth and phenology since 1960: A modeling approach, *Global and Planetary Change*, 143, 162–174, <https://doi.org/10.1016/j.gloplacha.2016.06.009>, 2016.
- Prasad, A. M., Iverson, L. R., and Liaw, A.: Newer classification and regression tree techniques: bagging and random forests for ecological prediction, *Ecosystems*, 9, 181–199, 2006.
- 870 Prinn, R. G., Weiss, R. F., Arduini, J., Arnold, T., DeWitt, H. L., Fraser, P. J., Ganesan, A. L., Gasore, J., Harth, C. M., and Hermansen, O.: History of chemically and radiatively important atmospheric gases from the Advanced Global Atmospheric Gases Experiment (AGAGE), *Earth System Science Data*, 10, 985–1018, 2018.
- R Core Team: R: a language and environment for statistical computing, version 3.0. 2. Vienna, Austria: R Foundation for Statistical Computing; 2013, 2019.
- 875 Rahimi, J., Haas, E., Grote, R., Kraus, D., Smerald, A., Laux, P., Goopy, J., and Butterbach-Bahl, K.: Beyond livestock carrying capacity in the Sahelian and Sudanian zones of West Africa, *Sci Rep*, 11, 22094, <https://doi.org/10.1038/s41598-021-01706-4>, 2021.
- Raich, J. W. and Potter, C. S.: *Global Patterns of CO₂ Emissions from Soils on a 0.5 Degree Grid Cell Basis*, 1996.
- Rastogi, M., Singh, S., and Pathak, H.: Emission of carbon dioxide from soil, *CURRENT SCIENCE*, 82, 9, 2002.
- 880 Ravishankara, A. R., Daniel, J. S., and Portmann, R. W.: Nitrous oxide (N₂O): the dominant ozone-depleting substance emitted in the 21st century, *science*, 326, 123–125, 2009.
- Ray, R. L., Griffin, R. W., Fares, A., Elhassan, A., Awal, R., Woldesenbet, S., and Risch, E.: Soil CO₂ emission in response to organic amendments, temperature, and rainfall, *Sci Rep*, 10, 5849, <https://doi.org/10.1038/s41598-020-62267-6>, 2020.

- 885 Reth, S., Reichstein, M., and Falge, E.: The effect of soil water content, soil temperature, soil pH-value and the root mass on soil CO₂ efflux – A modified model, *Plant Soil*, 268, 21–33, <https://doi.org/10.1007/s11104-005-0175-5>, 2005.
- Rey, A., Oyonarte, C., Morán-López, T., Raimundo, J., and Pegoraro, E.: Changes in soil moisture predict soil carbon losses upon rewetting in a perennial semiarid steppe in SE Spain, *Geoderma*, 287, 135–146, 2017.
- Robertson, G. P. and Paul, E. A.: Decomposition and soil organic matter dynamics, in: *Methods in ecosystem science*, Springer, 104–116, 2000.
- 890 Saikawa, E., Prinn, R. G., Dlugokencky, E., Ishijima, K., Dutton, G. S., Hall, B. D., Langenfelds, R., Tohjima, Y., Machida, T., Manizza, M., Rigby, M., O’Doherty, S., Patra, P. K., Harth, C. M., Weiss, R. F., Krummel, P. B., van der Schoot, M., Fraser, P. J., Steele, L. P., Aoki, S., Nakazawa, T., and Elkins, J. W.: Global and regional emissions estimates for N₂O, *Atmos. Chem. Phys.*, 14, 4617–4641, <https://doi.org/10.5194/acp-14-4617-2014>, 2014.
- 895 Shcherbak, I., Millar, N., and Robertson, G. P.: Global metaanalysis of the nonlinear response of soil nitrous oxide (N₂O) emissions to fertilizer nitrogen, *Proceedings of the National Academy of Sciences*, 111, 9199–9204, 2014.
- Signor, D. and Cerri, C. E. P.: Nitrous oxide emissions in agricultural soils: a review, *Pesquisa Agropecuária Tropical*, 43, 322–338, 2013.
- Smith, K. A., Ball, T., Conen, F., Dobbie, K. E., Massheder, J., and Rey, A.: Exchange of greenhouse gases between soil and atmosphere: interactions of soil physical factors and biological processes, *European journal of soil science*, 54, 779–791, 2003.
- 900 Sobol, I. M.: Global sensitivity indices for nonlinear mathematical models and their Monte Carlo estimates, *Mathematics and computers in simulation*, 55, 271–280, 2001.
- Soussana, J.-F., Tallec, T., and Blanfort, V.: Mitigating the greenhouse gas balance of ruminant production systems through carbon sequestration in grasslands, *Animal*, 4, 334–350, 2010.
- 905 Swinnen, E., Toté, C., and Van Hoolst, R.: ALGORITHM THEORETHICAL BASIS DOCUMENT DRY MATTER PRODUCTIVITY (DMP). GROSS DRY MATTER PRODUCTIVITY (GDMP), in: *Copernicus Global Land Operations” Vegetation and Energy”*, 2022.
- Takakai, F., Morishita, T., Hashidoko, Y., Darung, U., Kuramochi, K., Dohong, S., Limin, S. H., and Hatano, R.: Effects of agricultural land-use change and forest fire on N₂O emission from tropical peatlands, Central Kalimantan, Indonesia, *Soil Science and Plant Nutrition*, 52, 662–674, 2006.
- 910 Thornton, P. K. and Herrero, M.: Adapting to climate change in the mixed crop and livestock farming systems in sub-Saharan Africa, *Nature Climate Change*, 5, 830–836, 2015.
- Tian, H., Chen, G., Lu, C., Xu, X., Ren, W., Zhang, B., Banger, K., Tao, B., Pan, S., Liu, M., Zhang, C., Bruhwiler, L., and Wofsy, S.: Global methane and nitrous oxide emissions from terrestrial ecosystems due to multiple environmental changes, *Ecosystem Health and Sustainability*, 1, 1–20, <https://doi.org/10.1890/EHS14-0015.1>, 2015.
- 915 Tian, H., Lu, C., Ciais, P., Michalak, A. M., Canadell, J. G., Saikawa, E., Huntzinger, D. N., Gurney, K. R., Sitch, S., Zhang, B., Yang, J., Bousquet, P., Bruhwiler, L., Chen, G., Dlugokencky, E., Friedlingstein, P., Melillo, J., Pan, S., Poulter, B., Prinn, R., Saunio, M., Schwalm, C. R., and Wofsy, S. C.: The terrestrial biosphere as a net source of greenhouse gases to the atmosphere, *Nature*, 531, 225–228, <https://doi.org/10.1038/nature16946>, 2016.

- 920 Tian, H., Yang, J., Lu, C., Xu, R., Canadell, J. G., Jackson, R. B., Arneeth, A., Chang, J., Chen, G., Ciais, P., Gerber, S., Ito, A., Huang, Y., Joos, F., Lienert, S., Messina, P., Olin, S., Pan, S., Peng, C., Saikawa, E., Thompson, R. L., Vuichard, N., Winiwarter, W., Zaehle, S., Zhang, B., Zhang, K., and Zhu, Q.: The Global N₂O Model Intercomparison Project, *Bulletin of the American Meteorological Society*, 99, 1231–1251, <https://doi.org/10.1175/BAMS-D-17-0212.1>, 2018.
- 925 Tian, H., Yang, J., Xu, R., Lu, C., Canadell, J. G., Davidson, E. A., Jackson, R. B., Arneeth, A., Chang, J., Ciais, P., Gerber, S., Ito, A., Joos, F., Lienert, S., Messina, P., Olin, S., Pan, S., Peng, C., Saikawa, E., Thompson, R. L., Vuichard, N., Winiwarter, W., Zaehle, S., and Zhang, B.: Global soil nitrous oxide emissions since the preindustrial era estimated by an ensemble of terrestrial biosphere models: Magnitude, attribution, and uncertainty, *Glob Change Biol*, 25, 640–659, <https://doi.org/10.1111/gcb.14514>, 2019.
- 930 Tian, H., Xu, R., Canadell, J. G., Thompson, R. L., Winiwarter, W., Suntharalingam, P., Davidson, E. A., Ciais, P., Jackson, R. B., Janssens-Maenhout, G., Prather, M. J., Regnier, P., Pan, N., Pan, S., Peters, G. P., Shi, H., Tubiello, F. N., Zaehle, S., Zhou, F., Arneeth, A., Battaglia, G., Berthet, S., Bopp, L., Bouwman, A. F., Buitenhuis, E. T., Chang, J., Chipperfield, M. P., Dangal, S. R. S., Dlugokencky, E., Elkins, J. W., Eyre, B. D., Fu, B., Hall, B., Ito, A., Joos, F., Krummel, P. B., Landolfi, A., Laruelle, G. G., Lauerwald, R., Li, W., Lienert, S., Maavara, T., MacLeod, M., Millet, D. B., Olin, S., Patra, P. K., Prinn, R. G., Raymond, P. A., Ruiz, D. J., van der Werf, G. R., Vuichard, N., Wang, J., Weiss, R. F., Wells, K. C., Wilson, C., Yang, J., and Yao, Y.: A comprehensive quantification of global nitrous oxide sources and sinks, *Nature*, 586, 248–256, <https://doi.org/10.1038/s41586-020-2780-0>, 2020.
- 935 Torres, C. M. M. E., Jacovine, L. A. G., Nolasco de Olivera Neto, S., Fraisse, C. W., Soares, C. P. B., de Castro Neto, F., Ferreira, L. R., Zanuncio, J. C., and Lemes, P. G.: Greenhouse gas emissions and carbon sequestration by agroforestry systems in southeastern Brazil, *Sci Rep*, 7, 16738, <https://doi.org/10.1038/s41598-017-16821-4>, 2017.
- 940 Touré, I., Ickowicz, A., Wane, A., Garba, I., and Gerber, P.: Systeme d’information sur le pastoralisme au Sahel. Atlas des evolutions des systemes pastoraux au Sahel 1970-2012, 2012.
- Tracol, Y., Mougin, E., Hiernaux, P., and Jarlan, L.: Testing a sahelian grassland functioning model against herbage mass measurements, *Ecological Modelling*, 193, 437–446, 2006.
- 945 Tucker, C., Brandt, M., Hiernaux, P., Kariryaa, A., Rasmussen, K., Small, J., Igel, C., Reiner, F., Melocik, K., Meyer, J., Sinno, S., Romero, E., Glennie, E., Fitts, Y., Morin, A., Pinzon, J., McClain, D., Morin, P., Porter, C., Loeffler, S., Kergoat, L., Issoufou, B.-A., Savadogo, P., Wigneron, J.-P., Poulter, B., Ciais, P., Kaufmann, R., Myneni, R., Saatchi, S., and Fensholt, R.: Sub-continental-scale carbon stocks of individual trees in African drylands, *Nature*, 615, 80–86, <https://doi.org/10.1038/s41586-022-05653-6>, 2023.
- Turner, M. D., McPeak, J. G., and Ayantunde, A.: The Role of Livestock Mobility in the Livelihood Strategies of Rural Peoples in Semi-Arid West Africa, *Human Ecology*, 42, 231–247, 2014.
- 950 Valentini, R., Arneeth, A., Bombelli, A., Castaldi, S., Cazzolla Gatti, R., Chevallier, F., Ciais, P., Grieco, E., Hartmann, J., and Henry, M.: A full greenhouse gases budget of Africa: synthesis, uncertainties, and vulnerabilities, *Biogeosciences*, 11, 381–407, 2014.
- 955 Verchot, L. V., Davidson, E. A., Cattânio, H., Ackerman, I. L., Erickson, H. E., and Keller, M.: Land use change and biogeochemical controls of nitrogen oxide emissions from soils in eastern Amazonia, *Global Biogeochemical Cycles*, 13, 31–46, 1999.
- Vezy, R., le Maire, G., Christina, M., Georgiou, S., Imbach, P., Hidalgo, H. G., Alfaro, E. J., Blitz-Frayret, C., Charbonnier, F., Lehner, P., Loustau, D., and Rouspard, O.: DynACof: A process-based model to study growth, yield and ecosystem services

of coffee agroforestry systems, *Environmental Modelling & Software*, 124, 104609, <https://doi.org/10.1016/j.envsoft.2019.104609>, 2020.

960 Warner, D. L., Bond-Lamberty, B., Jian, J., Stell, E., and Vargas, R.: Spatial Predictions and Associated Uncertainty of Annual Soil Respiration at the Global Scale, *Global Biogeochemical Cycles*, 33, 1733–1745, <https://doi.org/10.1029/2019GB006264>, 2019.

Webb, H., Barnes, N., Powell, S., and Jones, C.: Does drone remote sensing accurately estimate soil pH in a spring wheat field in southwest Montana?, *Precision Agric*, 22, 1803–1815, <https://doi.org/10.1007/s11119-021-09812-z>, 2021.

965 Xu, M. and Shang, H.: Contribution of soil respiration to the global carbon equation, *Journal of plant physiology*, 203, 16–28, 2016.

Xu, R., Tian, H., Pan, S., Dangal, S. R., Chen, J., Chang, J., Lu, Y., Skiba, U. M., Tubiello, F. N., and Zhang, B.: Increased nitrogen enrichment and shifted patterns in the world's grassland: 1860–2016, *Earth System Science Data*, 11, 175–187, 2019.

970 Yao, Y., Tian, H., Shi, H., Pan, S., Xu, R., Pan, N., and Canadell, J. G.: Increased global nitrous oxide emissions from streams and rivers in the Anthropocene, *Nature Climate Change*, 10, 138–142, 2020.